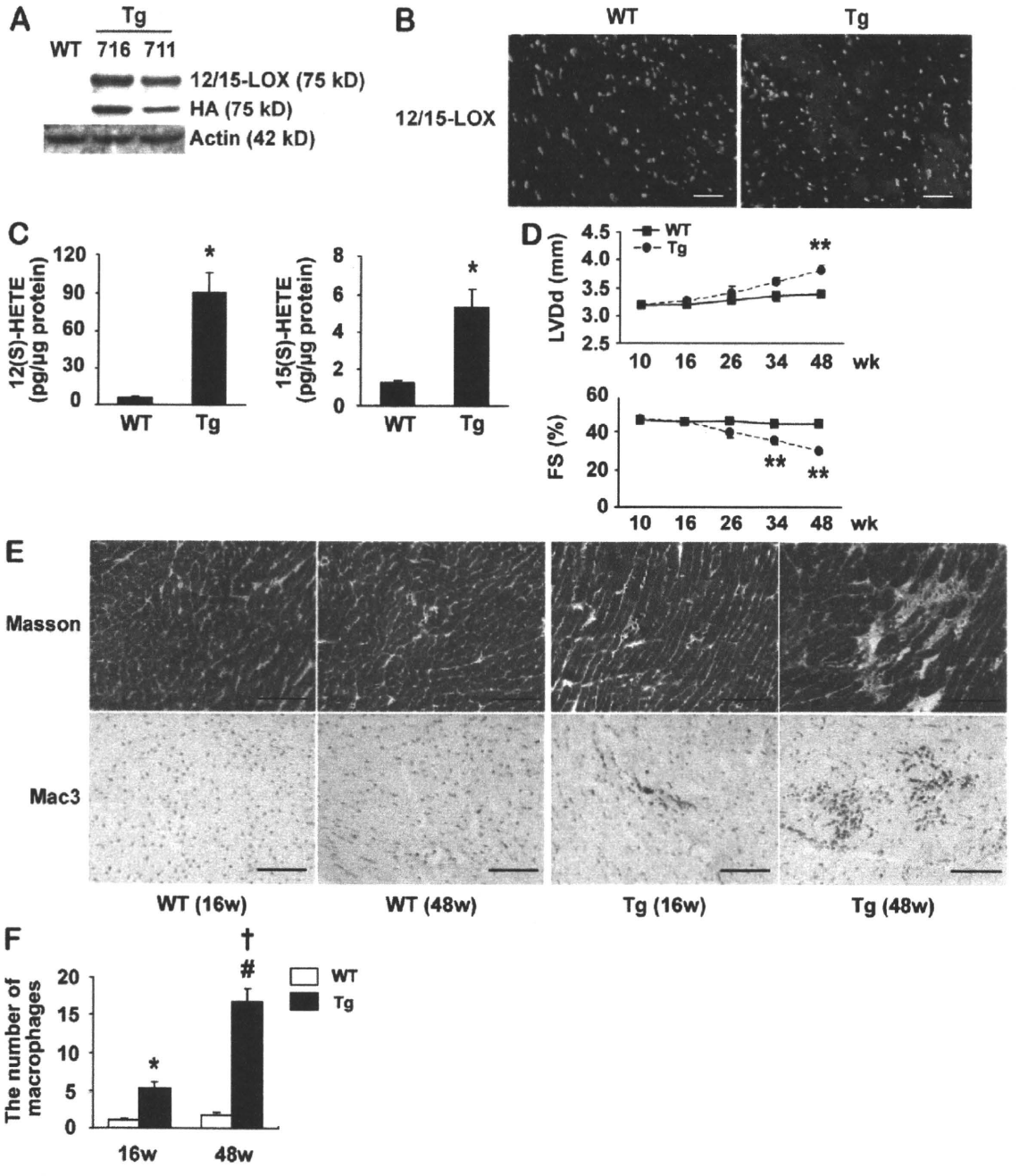

Figure 2. Increased expression of 12/15-LOX causes heart failure. (A) Western blot analysis of 12/15-LOX expression in the hearts of WT and *Alox15* transgenic (Tg) mice using anti-12/15-LOX antibody (12/15-LOX) or anti-HA antibody (HA). (B) Immunohistochemistry for 12/15-LOX (red) in the hearts of WT and *Alox15* transgenic mice. Nuclei were stained with DAPI (blue). Bars, 40 μm. Results in A and B are representative of three independent experiments. (C) 12/15(S)-HETE levels in the hearts of WT and *Alox15* transgenic mice. (D) Echocardiographic findings in WT and transgenic mice. The LVDd was increased and left ventricular FS was decreased in *Alox15* transgenic mice compared with their WT littermates. These changes observed in the transgenic animals showed progression with aging. *, $P < 0.05$; **, $P < 0.01$ versus WT. Results in C and D represent the mean ± SEM of three independent experiments. C, $n = 6$; D, $n = 14$. (E) Masson trichrome staining (top) and immunohistochemistry for Mac3 (bottom) in the hearts of WT and transgenic mice at the ages of 16 wk (16w) and 48 wk (48w). Cardiac fibrosis was increased in *Alox15* transgenic mice, and this fibrosis progressed with advancing age and was associated with infiltration of macrophages. Bars, 100 μm. Results are representative of three independent experiments. (F) The number of Mac3-positive cells in the hearts of WT and transgenic mice at the ages of 16 wk (16w) and 48 wk (48w). *, $P < 0.01$ versus WT (16w); #, $P < 0.01$ versus WT (48w); †, $P < 0.01$ versus transgenic (16w). Results represent the mean ± SEM of three independent experiments; $n = 7$.

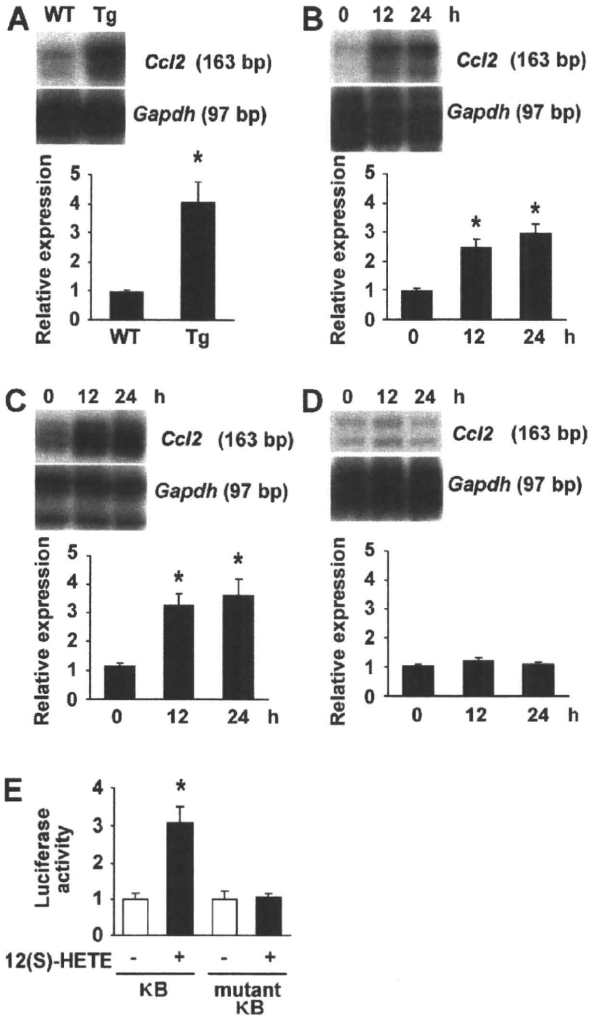

Figure 3. 12/15-LOX up-regulates MCP-1 expression. (A) Expression of *Ccl2* (MCP-1) was examined in the hearts of WT and *12/15-LOX* transgenic (Tg) mice by the ribonuclease protection assay. The graph indicates relative expression of *Ccl2*. Cardiac expression of *Ccl2* was significantly greater in *Alox15* transgenic mice than in WT mice. *, $P < 0.05$ versus WT. Results represent the mean ± SEM of three independent experiments; $n = 6$. (B–D) Cardiac fibroblasts (B), endothelial cells (C), and cardiomyocytes (D) were treated with 5×10^{-7} M 12(S)-HETE for the indicated times (0–24 h), and expression of *Ccl2* was examined by the ribonuclease protection assay. Graphs display relative expression of *Ccl2*. Incubation with 12(S)-HETE increased *Ccl2* expression by cardiac fibroblasts and endothelial cells. *, $P < 0.01$ versus time 0. Results represent mean ± SEM of four independent experiments; $n = 4$ for B and C; $n = 7$ for D. (E) The luciferase reporter gene plasmid containing the κB binding site was transfected into COS7 cells, which were cultured in the absence or presence of 5×10^{-7} M 12(S)-HETE. The luciferase assay was performed 12 h later. A reporter plasmid containing the mutant κB binding site was used as the negative control. Incubation of cells with 12(S)-HETE significantly increased the activity of nuclear factor κB. *, $P < 0.01$ versus 12(S)-HETE (−)/κB. Results represent the mean ± SEM of five independent experiments; $n = 6$.

histological examination and echocardiography demonstrated that injection of this plasmid reduced the myocardial infiltration of macrophages in *Alox15* transgenic mice, as well as preventing systolic dysfunction and left ventricular dilatation (Fig. 4, B and C). These results suggested that 12/15-LOX induces cardiac dysfunction by up-regulation of MCP-1 expression in the heart.

Cardiac expression of 12/15-LOX is up-regulated during pressure overload

To further investigate the role of 12/15-LOX in heart failure, we examined its cardiac expression in WT mice with severe transverse aortic constriction (TAC). In this model, cardiac hypertrophy gradually progresses to reach a peak on day 7 after TAC and then decreases afterward (not depicted). FS was preserved until day 7 but was significantly decreased on day 14 along with left ventricular dilatation (Fig. 5 A). Cardiac expression of *Alox15* was significantly up-regulated after TAC (Fig. 5 B), and the production of both 12(S)-HETE and 15(S)-HETE was increased in the heart (Fig. 5 C). Histological examination demonstrated an increase in the expression of 12/15-LOX by cardiomyocytes after TAC (Fig. 6 A and Fig. S3).

We next created *Alox15*-deficient mice with TAC and compared them to WT TAC mice. The increase of 12(S)-HETE and 15(S)-HETE production after TAC was markedly attenuated by disruption of *Alox15* (Fig. 6). Disruption of *Alox15* also significantly improved systolic dysfunction and prevented left ventricular dilatation in the presence of chronic pressure overload without any change of blood pressure (Fig. 5 A and Fig. S4), indicating that 12/15-LOX has an important role in the induction of cardiac dysfunction by pressure overload. To examine whether *Alox15* deficiency could inhibit cardiac inflammation, we assessed the expression of *Cd2* and a macrophage marker (Cd68) in the heart after TAC. Expression of both genes was increased by about threefold at 14 d after TAC. The increase of *Cd2* and *Cd68* expression was significantly inhibited by disruption of *Alox15* (Fig. 6 C), suggesting that this gene has a crucial role in the development of heart failure by promoting cardiac inflammation.

DISCUSSION

We demonstrated a crucial role of 12/15-LOX–induced inflammation in the development of heart failure. Activation of this enzyme has been shown to promote neuronal death, whereas inhibition of 12/15-LOX protects against brain damage caused by oxidative stress or ischemia by inhibiting neuronal death (Lebeau et al., 2004; Jin et al., 2008; Seiler et al., 2008). In contrast, treatment with 12(S)-HETE does not induce the apoptosis of cultured cardiomyocytes (unpublished data). Indeed, few apoptotic cardiomyocytes were detected in the hearts of *Alox15* transgenic mice even after the onset of systolic dysfunction (unpublished data). Instead, these mice showed an increase of macrophages infiltrating into the myocardium, which was associated with cardiac fibrosis and systolic dysfunction. Our findings suggested that MCP-1 may

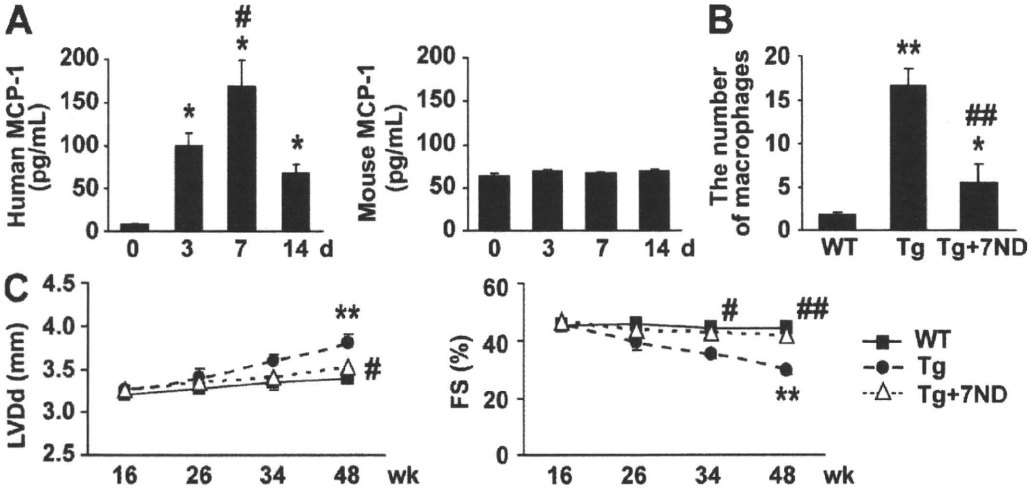

Figure 4. Inhibition of MCP-1 prevents cardiac dysfunction in *Alox15* transgenic animals. (A) The plasma levels of 7ND (human MCP-1) and murine MCP-1 were determined by ELISA at the indicated times after introduction of the 7ND expression vector. The plasma level of human MCP-1 was significantly increased after injection of the 7ND plasmid. *, $P < 0.01$ versus day 0; #, $P < 0.01$ versus day 3. Results represent the mean ± SEM of three independent experiments; $n = 5$. (B) Number of Mac3-positive cells in the hearts of WT mice, transgenic (Tg) mice, and transgenic mice treated with 7ND (Tg + 7ND). Injection of the 7ND plasmid reduced the myocardial infiltration of macrophages in *Alox15* transgenic mice. (C) Echocardiographic findings in WT mice, transgenic mice, and transgenic mice treated with 7ND (Tg + 7ND). Injection of the 7ND plasmid prevented systolic dysfunction and left ventricular dilatation in *Alox15* transgenic mice. *, $P < 0.05$; **, $P < 0.01$ versus WT; #, $P < 0.05$; ##, $P < 0.01$ versus transgenic. Results represent mean ± SEM of three independent experiments. B, $n = 7$; C, $n = 10$–14.

have a major role in promoting cardiac inflammation in *Alox15* transgenic mice because its inhibition almost completely abolished the accumulation of macrophages and prevented systolic dysfunction. We also showed that 12/15-LOX induces up-regulation of MCP-1 expression in the setting of pressure overload, thereby increasing cardiac inflammation and leading to systolic dysfunction. Consistent with our findings, inhibition of MCP-1 has been reported to attenuate

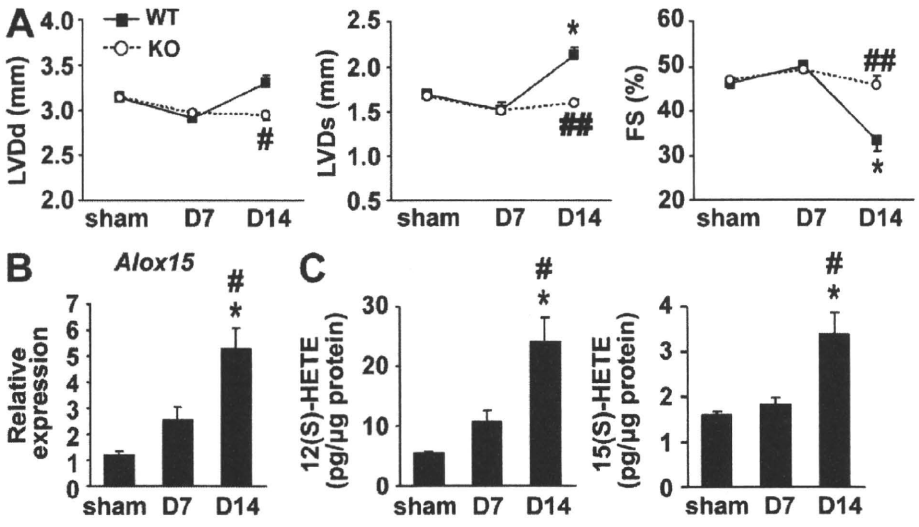

Figure 5. Cardiac expression of 12/15-LOX is up-regulated during pressure overload. (A) Echocardiographic findings in WT and *Alox15*-deficient (KO) mice on day 7 (D7) and day 14 (D14) after TAC surgery. FS was preserved until day 7 but was significantly decreased on day 14 along with left ventricular dilatation in WT mice. Disruption of *Alox15* (KO) significantly improved systolic dysfunction and prevented left ventricular dilatation caused by chronic pressure overload. LVDs, left ventricular systolic dimension; sham, sham operation. *, $P < 0.01$ versus sham; #, $P < 0.05$; ##, $P < 0.01$ versus WT. Results represent the mean ± SEM of three independent experiments; $n = 10$. (B and C) *Alox15* expression (B) and the 12/15(S)-HETE level (C) were examined in the hearts of WT mice on day 7 (D7) and day 14 (D14) after TAC surgery by real-time PCR and ELISA, respectively. Cardiac expression of 12/15-LOX was significantly up-regulated after TAC, and production of both 12(S)-HETE and 15(S)-HETE was increased in the heart. *, $P < 0.01$ versus sham; #, $P < 0.01$ versus D7. Results represent the mean ± SEM of three independent experiments; $n = 6$.

myocardial inflammation, fibrosis, and cardiac dysfunction induced by chronic pressure overload (Kuwahara et al., 2004). It has also been reported that transgenic animals with cardiac expression of MCP-1 develop myocardial fibrosis and systolic dysfunction (Kolattukudy et al., 1998). In agreement with our in vitro data, it has been reported that MCP-1 expression is up-regulated in vascular endothelial cells and fibroblasts by pressure overload (Kuwahara et al., 2004). Collectively, these

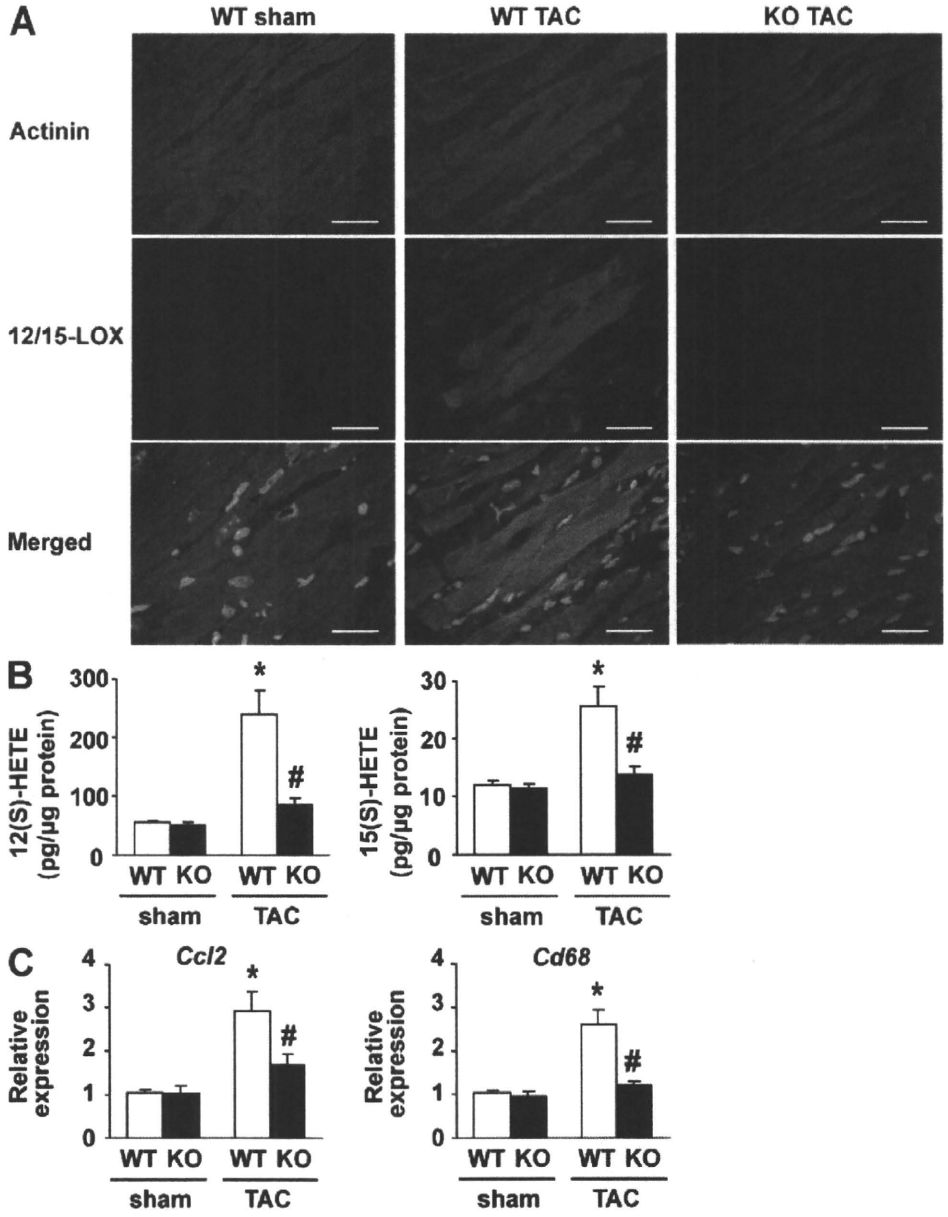

Figure 6. Disruption of *Alox15* attenuates cardiac inflammation during pressure overload. (A) Double immunostaining for 12/15-LOX (red) and actinin (green) in the hearts of sham-operated WT mice (WT sham), WT mice with TAC (WT TAC), and *Alox15*-deficient mice with TAC (KO TAC). Increased expression of 12/15-LOX was observed in cardiomyocytes after TAC in WT mice but not KO mice. Nuclei were stained with DAPI (blue). Bars, 20 μm. Results are representative of four independent experiments. (B) 12/15(S)-HETE levels were examined in the hearts of WT and *Alox15*-deficient (KO) mice after sham surgery or TAC. The increase of 12(S)-HETE and 15(S)-HETE production after TAC was markedly attenuated in *Alox15*-deficient mice (KO). *, $P < 0.01$ versus WT sham; #, $P < 0.01$ versus WT TAC. Results represent the mean ± SEM of three independent experiments; $n = 6–8$. (C) Expression of *Ccl2* (MCP-1) and *Cd68* was examined in the hearts of WT and *Alox15*-deficient (KO) mice after sham surgery or TAC. Expression of both genes was increased by about threefold at 14 d after TAC. This increase of expression was significantly inhibited by disruption of *Alox15*. *, $P < 0.01$ versus WT sham; #, $P < 0.01$ versus WT TAC. Results represent the mean ± SEM of three independent experiments; $n = 6–8$.

results indicate that chronic pressure overload increases the expression of 12/15-LOX, which then causes heart failure by promoting cardiac inflammation and fibrosis.

Target gene disruption or overexpression of 12/15-LOX in mice with a genetic background of apolipoprotein E or low-density lipoprotein receptor deficiency has shown that this enzyme may have a role in atherogenesis. The data indirectly support a role for 12/15-LOX in the oxidative modification of low-density lipoprotein. Consistent with our results, recent evidence suggests that 12/15-LOX plays a crucial role in the regulation of proinflammatory molecules and that this regulatory activity of 12/15-LOX may be important for linking 12/15-LOX activation to atherogenesis. For example, 12(S)-HETE increases the expression of MCP-1, interleukin 6, tumor necrosis factor α, and adhesion molecules by macrophages and vascular cells (Bolick et al., 2005, 2006; Wen et al., 2007, 2008; Dwarakanath et al., 2008), and these changes are partly mediated by activation of nuclear factor κB (Bolick et al., 2005, 2006; Dwarakanath et al., 2008). Disruption of 12/15-LOX has also been shown to attenuate airway allergic inflammation by modulating the expression of proinflammatory cytokines (Andersson et al., 2008).

The mechanism of 12/15-LOX activation in the failing heart is unclear. We previously demonstrated that mismatch between the number of capillaries and the size of cardiomyocytes occurs during the development of cardiac hypertrophy, leading to myocardial hypoxia and systolic dysfunction (Sano et al., 2007). Because exposure of cultured cardiomyocytes to hypoxia up-regulates 12/15-LOX expression (unpublished data), a hypoxic state might be one reason for the induction of 12/15-LOX in the failing heart. This concept is supported by previous results that hypoxia up-regulates 12/15-LOX expression in the lungs and the brain (Bernaudin et al., 2002; Zhu et al., 2003a). Moreover, we have found that 12/15-LOX expression is significantly up-regulated in the heart after myocardial infarction (unpublished data). There are putative binding elements for CCAAT/enhancer binding proteins and nuclear factor κB within the promoter region of the *Alox15* gene (unpublished data), and both of these molecules are known to be activated by hypoxia (Cummins and Taylor, 2005).

Inflammation has an important role in the pathogenesis and progression of many forms of heart failure, and biomarkers of inflammation have become the subject of intense investigation. In the Framingham Heart Study, an increase of C-reactive protein (as well as inflammatory cytokines such as interleukin 6 and tumor necrosis factor α) was found to identify asymptomatic older persons in the community with a high risk of developing heart failure in the future (Braunwald, 2008). Multivariate analysis has shown that an increase of C-reactive protein is an independent predictor of adverse outcomes in patients with acute or chronic heart failure (Anand et al., 2005), suggesting that heart failure is closely associated with systemic inflammation. Because metabolites of 12/15-LOX may have a role in vascular inflammation, insulin resistance, and renal dysfunction (Natarajan and Nadler, 2004; Kuhn and O'Donnell, 2006), activation of 12/15-LOX in the failing heart could induce systemic inflammation and have a detrimental effect on other inflammatory diseases such as atherosclerosis, metabolic syndrome, and nephropathy. Conversely, inhibition of 12/15-LOX could be an attractive new strategy for the treatment of heart failure, as well as various other inflammatory conditions.

MATERIALS AND METHODS

Animal models. All of the experimental protocols were approved by Chiba University review board. Male Dahl salt-sensitive (DS) rats were purchased from SLC. The rats were fed a low-sodium diet until the age of 6 wk and then a high-sodium diet (8% NaCl) throughout the experimental period. In this model, marked cardiac hypertrophy developed and left ventricular systolic function was impaired at 17 wk of age. Accordingly, DS rats were sacrificed for gene chip analysis at 17 wk. All of the DS rats given a high-sodium diet showed signs of heart failure such as rapid and labored respiration and diffuse left ventricular hypokinesis on echocardiography at the time of sacrifice. Other DS rats were fed a low-salt diet (0.3% NaCl) as a control group.

We generated transgenic mice on a C57BL/6 background that expressed 12/15-LOX in cardiomyocytes under the control of the α–cardiac myosin heavy chain (α-MHC) promoter. A mouse *Alox15* complementary DNA (cDNA) fragment (gift from C.D. Funk, University of Pennsylvania, Philadelphia, PA) fused with the HA tag was subcloned into the α-MHC promoter vector. The transgene was identified by genomic PCR with transgene-specific oligonucleotide primers (5′-CCACACCAGAAATGACAGAC-3′ and 5′-GCGGGCAGGGAGACAAGTAG-3′) and by Southern blot analysis. Two independent lines of *Alox15* transgenic mice (lines 711 and 716) were obtained. The cardiac phenotype was similar in both lines of transgenic animals. WT littermates were used as the control for all experiments.

Alox15-deficient mice on a C57BL/6 background were purchased from The Jackson Laboratory. WT littermates served as a control for all experiments. TAC was performed as described previously (Sano et al., 2007) on 10–11-wk-old male mice. Sham-operated mice underwent the same procedure without aorta constriction.

An expression vector encoding mutant human MCP-1 with deletion of N-terminal amino acids (7ND plasmid) was prepared as described elsewhere (Hayashidani et al., 2003). Under anesthesia, mice received an injection of 100 μg of either the empty vector or the 7ND plasmid in PBS into the bilateral tibial muscles using a 27-gauge needle fitted with a plastic collar that limited muscle penetration to ~5 mm. Injection was performed every 2 wk from 10 wk until 48 wk of age. To increase the efficiency of gene transfection, 100 μl of the myotoxic agent bupivacaine (0.25% wt/vol) was injected into the muscles 3 d before transfection. Transfection of 7ND leads to an increase of mutant MCP-1 in the blood, as indicated by elevation of its plasma concentration after 14 d. The circulating mutant MCP-1 binds to the receptor for MCP-1 (chemokine receptor 2) on target cells and effectively blocks MCP-1 signaling (Ni et al., 2001; Hayashidani et al., 2003).

Physiological and histological analysis. Echocardiography was performed with a Vevo 770 High Resolution Imaging System (Visual Sonics Inc.). To minimize variation of the data, the heart rate was ~500-600 beats per minute when cardiac function was assessed. The peak systolic blood pressure was recorded by a photoelectric pulse devise (Blood Pressure Meter BP-98A; Softron Co. Ltd.) placed on the tails of unanesthetized mice. Under anesthesia, a micropressure transducer with an outer diameter of 0.42 mm (Samba 201 control unit and Samba Preclin 420 transducer; Samba Sensors AB) was introduced into the right carotid artery. Pressure signals were recorded with a MacLab 3.6/s data acquisition system (AD Instruments) at a sampling rate of 2,000 Hz. 4-μm frozen cross sections of the heart were fixed in 4% paraformaldehyde and subjected to Masson trichrome staining or immunohistochemistry for Mac3 (BD). Digital photographs were taken at 400× magnification of 25 random fields from each heart, and the number of Mac3-positive cells was counted in each field. The frozen cardiac cross sections

were also stained with antibodies for 12/15-LOX (Cayman Chemical) and actinin (Sigma-Aldrich).

DNA chip analysis. 10 µg of total RNA was extracted from the left ventricles of rats by the Li-Urea method and was used to synthesize biotin-labeled cRNA, which was then hybridized to a high-density oligonucleotide array (Gene Chip U34A array; Affymetrix) according to the previously published protocol (Ishii et al., 2000). The array contains probe sets for ~8,800 genes and ESTs, which were selected from Build 34 of the UniGene Database (created from GenBank 107/dbEST 11/18/98). GeneChip 3.3 software (Affymetrix) was used to calculate the mean difference for each probe on the array, which showed the intensity of gene expression defined by Affymetrix using their algorithm. The mean difference has been shown to quantitatively reflect the abundance of a particular mRNA in a population. The data were deposited in GEO (GSM406556, GSM406557, and GSE16199).

RNA analysis. Total RNA was isolated from the hearts of mice with RNAZol-B (Molecular Research Center, Cincinnati, OH) and the ribonuclease protection assay (RiboQuant; BD) was performed according to the manufacturer's instructions. For Northern blot analysis, 30 µg of total RNA was separated on formaldehyde denaturing gel and transferred to a nylon membrane (GE Healthcare). Then the blot was hybridized with radiolabeled *Alox15* cDNA probe using Quickhyb hybridization solution (Agilent Technologies) according to the manufacturer's instructions. Rat *Alox15* cDNA fragment was a gift from T. Yoshimoto (Kanazawa University Graduate School of Medical Science, Kanazawa, Japan). Mouse *Alox12* cDNA fragment was a gift from C.D. Funk. Real-time PCR was performed using a LightCycler (Roche) with the Taqman Universal Probe Library and the Light Cycler Master (Roche) according to the manufacturer's instructions.

Western blot analysis. Whole cell lysates were prepared in lysis buffer (10 mM Tris-HCl, pH 8, 140 mM NaCl, 5 mM EDTA, 0.025% NaN_3, 1% Triton X-100, 1% deoxycholate, 0.1% SDS, 1 mM PMSF, 5 µg/ml leupeptin, 2 µg/ml aprotinin, 50 mM NaF, and 1 mM $Na2VO_3$). 40–50 µg of the lysates were resolved by SDS-PAGE (PAGE). Then proteins were transferred to a nitrocellulose membrane (GE Healthcare), which was incubated with the primary antibody, followed by anti–rabbit or anti–mouse immunoglobulin G conjugated with horseradish peroxidase (Jackson ImmunoResearch Laboratories). Specific proteins were detected by using enhanced chemiluminescence (GE Healthcare). The primary antibodies used for Western blotting were as follows: anti-HA antibody (Santa Cruz Biotechnology, Inc.), anti–12/15-LOX antibody (Cayman Chemical), and anti-actin antibody (Sigma-Aldrich). ELISA was performed according to the manufacturer's instructions to examine the levels of 12(S)-HETE, 15(S)-HETE (Assay Designs), human MCP-1, and mouse MCP-1 (Invitrogen).

Cell culture. Neonatal Wistar rats were purchased from Takasugi Experimental Animal Supply. Cardiomyocytes and cardiac fibroblasts were prepared from these neonatal rats and cultured as described previously (Sano et al., 2007). Human umbilical vein endothelial cells (BioWhittaker; Lonza) were cultured according to the manufacturer's instructions.

Luciferase assay. 1 µg of the reporter gene plasmid was transfected into COS7 cells at 24 h before the luciferase assay. 0.1 µg of the control vector encoding *Renilla* luciferase was cotransfected as an internal control. The assay was performed using a dual luciferase reporter assay system (Promega) according to the manufacturer's instructions. p55-A2-Luc (the luciferase reporter gene containing the κB binding site) was a gift from T. Fujita (The Tokyo Metropolitan Institute of Medical Science, Tokyo, Japan; Fujita et al., 1993).

Statistical analysis. Data are shown as the mean ± SEM. Multiple group comparison was performed by one-way ANOVA, followed by Bonferroni's test for comparison of means. Comparisons between two groups were done with the two-tailed unpaired Student's *t* test or two-way ANOVA. In all analyses, $P < 0.05$ was considered statistically significant.

Online supplemental material. Fig. S1 depicts *Alox15* transgenic animal data. Fig. S2 shows MCP-1 levels after treatment with 7ND. Fig. S3 shows a negative control of immunohistochemistry for 12/15-LOX. Fig. S4 shows blood pressure of *Alox15*-deficient mice. Table S1 summarizes the microarray data. Online supplemental material is available at http://www.jem.org/cgi/content/full/jem.20082596/DC1.

We thank Dr. C. Funk, Dr. T. Yoshimoto, and Dr. T. Fujita for reagents and E. Fujita, R. Kobayashi, Y. Ishiyama, and M. Ikeda for technical support.

This work was supported by a Grant-in-Aid for Scientific Research from the Ministry of Education, Science, Sports, and Culture, and Health and Labor Sciences Research Grants (to I. Komuro), a Grant-in-Aid for Scientific Research from the Ministry of Education, Culture, Sports, Science and Technology of Japan, grants from the Suzuken Memorial Foundation, the Japan Diabetes Foundation, the Ichiro Kanehara Foundation, the Tokyo Biochemical Research Foundation, and the Cell Science Research Foundation (to T. Minamino), grants from the Takeda Science Foundation and the Japan Foundation of Applied Enzymology (to T. Minamino and H. Toko), and Sakakibara Memorial research Grant from the Japan Research Promotion Society for Cardiovascular Disease (to H. Toko).

The authors declare no competing financial interests.

Submitted: 17 November 2008
Accepted: 29 May 2009

REFERENCES

Anand, I.S., R. Latini, V.G. Florea, M.A. Kuskowski, T. Rector, S. Masson, S. Signorini, P. Mocarelli, A. Hester, R. Glazer, and J.N. Cohn. 2005. C-reactive protein in heart failure: prognostic value and the effect of valsartan. *Circulation.* 112:1428–1434.

Andersson, C.K., H.E. Claesson, K. Rydell-Tormanen, S. Swedmark, A. Hallgren, and J.S. Erjefalt. 2008. Mice lacking 12/15-lipoxygenase have attenuated airway allergic inflammation and remodeling. *Am. J. Respir. Cell Mol. Biol.* 39:648–656.

Bernaudin, M., Y. Tang, M. Reilly, E. Petit, and F.R. Sharp. 2002. Brain genomic response following hypoxia and re-oxygenation in the neonatal rat. Identification of genes that might contribute to hypoxia-induced ischemic tolerance. *J. Biol. Chem.* 277:39728–39738.

Bleich, D., S. Chen, B. Zipser, D. Sun, C.D. Funk, and J.L. Nadler. 1999. Resistance to type 1 diabetes induction in 12-lipoxygenase knockout mice. *J. Clin. Invest.* 103:1431–1436.

Bolick, D.T., A.W. Orr, A. Whetzel, S. Srinivasan, M.E. Hatley, M.A. Schwartz, and C.C. Hedrick. 2005. 12/15-lipoxygenase regulates intercellular adhesion molecule-1 expression and monocyte adhesion to endothelium through activation of RhoA and nuclear factor-kappaB. *Arteriosder. Thromb. Vasc. Biol.* 25:2301–2307.

Bolick, D.T., S. Srinivasan, A. Whetzel, L.C. Fuller, and C.C. Hedrick. 2006. 12/15 lipoxygenase mediates monocyte adhesion to aortic endothelium in apolipoprotein E-deficient mice through activation of RhoA and NF-kappaB. *Arteriosder. Thromb. Vasc. Biol.* 26:1260–1266.

Braunwald, E. 2008. Biomarkers in heart failure. *N. Engl. J. Med.* 358:2148–2159.

Chen, X.S., U. Kurre, N.A. Jenkins, N.G. Copeland, and C.D. Funk. 1994. cDNA cloning, expression, mutagenesis of C-terminal isoleucine, genomic structure, and chromosomal localizations of murine 12-lipoxygenases. *J. Biol. Chem.* 269:13979–13987.

Cummins, E.P., and C.T. Taylor. 2005. Hypoxia-responsive transcription factors. *Pflugers Arch.* 450:363–371.

Cyrus, T., J.L. Witztum, D.J. Rader, R. Tangirala, S. Fazio, M.F. Linton, and C.D. Funk. 1999. Disruption of the 12/15-lipoxygenase gene diminishes atherosclerosis in apo E-deficient mice. *J. Clin. Invest.* 103:1597–1604.

Cyrus, T., D. Pratico, L. Zhao, J.L. Witztum, D.J. Rader, J. Rokach, G.A. FitzGerald, and C.D. Funk. 2001. Absence of 12/15-lipoxygenase expression decreases lipid peroxidation and atherogenesis in apolipoprotein e-deficient mice. *Circulation.* 103:2277–2282.

Dwarakanath, R.S., S. Sahar, L. Lanting, N. Wang, M.B. Stemerman, R. Natarajan, and M.A. Reddy. 2008. Viral vector-mediated

12/15-lipoxygenase overexpression in vascular smooth muscle cells enhances inflammatory gene expression and migration. *J. Vasc. Res.* 45:132–142.

Egashira, K. 2003. Molecular mechanisms mediating inflammation in vascular disease: special reference to monocyte chemoattractant protein-1. *Hypertension.* 41:834–841.

Fujita, T., G.P. Nolan, H.C. Liou, M.L. Scott, and D. Baltimore. 1993. The candidate proto-oncogene bcl-3 encodes a transcriptional coactivator that activates through NF-kappa B p50 homodimers. *Genes Dev.* 7:1354–1363.

Garg, R., and S. Yusuf. 1995. Overview of randomized trials of angiotensin-converting enzyme inhibitors on mortality and morbidity in patients with heart failure. Collaborative group on ACE inhibitor trials. *JAMA.* 273:1450–1456.

George, J., A. Afek, A. Shaish, H. Levkovitz, N. Bloom, T. Cyrus, L. Zhao, C.D. Funk, E. Sigal, and D. Harats. 2001. 12/15-Lipoxygenase gene disruption attenuates atherogenesis in LDL receptor-deficient mice. *Circulation.* 104:1646–1650.

Goldstein, S. 2002. Benefits of beta-blocker therapy for heart failure: weighing the evidence. *Arch. Intern. Med.* 162:641–648.

Hatley, M.E., S. Srinivasan, K.B. Reilly, D.T. Bolick, and C.C. Hedrick. 2003. Increased production of 12/15 lipoxygenase eicosanoids accelerates monocyte/endothelial interactions in diabetic db/db mice. *J. Biol. Chem.* 278:25369–25375.

Hayashidani, S., H. Tsutsui, T. Shiomi, M. Ikeuchi, H. Matsusaka, N. Suematsu, J. Wen, K. Egashira, and A. Takeshita. 2003. Anti-monocyte chemoattractant protein-1 gene therapy attenuates left ventricular remodeling and failure after experimental myocardial infarction. *Circulation.* 108:2134–2140.

Ishii, M., S. Hashimoto, S. Tsutsumi, Y. Wada, K. Matsushima, T. Kodama, and H. Aburatani. 2000. Direct comparison of GeneChip and SAGE on the quantitative accuracy in transcript profiling analysis. *Genomics.* 68:136–143.

Jin, G., K. Arai, Y. Murata, S. Wang, M.F. Stins, E.H. Lo, and K. van Leyen. 2008. Protecting against cerebrovascular injury: contributions of 12/15-lipoxygenase to edema formation after transient focal ischemia. *Stroke.* 39:2538–2543.

Kolattukudy, P.E., T. Quach, S. Bergese, S. Breckenridge, J. Hensley, R. Altschuld, G. Gordillo, S. Klenotic, C. Orosz, and J. Parker-Thornburg. 1998. Myocarditis induced by targeted expression of the MCP-1 gene in murine cardiac muscle. *Am. J. Pathol.* 152:101–111.

Kudo, I., and M. Murakami. 2002. Phospholipase A2 enzymes. *Prostaglandins Other Lipid Mediat.* 68-69:3–58.

Kuhn, H., and V.B. O'Donnell. 2006. Inflammation and immune regulation by 12/15-lipoxygenases. *Prog. Lipid Res.* 45:334–356.

Kuwahara, F., H. Kai, K. Tokuda, M. Takeya, A. Takeshita, K. Egashira, and T. Imaizumi. 2004. Hypertensive myocardial fibrosis and diastolic dysfunction: another model of inflammation? *Hypertension.* 43:739–745.

Lebeau, A., F. Terro, W. Rostene, and D. Pelaprat. 2004. Blockade of 12-lipoxygenase expression protects cortical neurons from apoptosis induced by beta-amyloid peptide. *Cell Death Differ.* 11:875–884.

Libby, P., and E. Braunwald. 2008. Braunwald's Heart Disease: a Textbook of Cardiovascular Medicine. Saunders/Elsevier, Philadelphia. 509 pp.

McDuffie, M., N.A. Maybee, S.R. Keller, B.K. Stevens, J.C. Garmey, M.A. Morris, E. Kropf, C. Rival, K. Ma, J.D. Carter, et al. 2008. Nonobese diabetic (NOD) mice congenic for a targeted deletion of 12/15-lipoxygenase are protected from autoimmune diabetes. *Diabetes.* 57:199–208.

McMurray, J.J. 1999. Major beta blocker mortality trials in chronic heart failure: a critical review. *Heart.* 82:IV14–IV22.

McNally, A.K., G.M. Chisolm III, D.W. Morel, and M.K. Cathcart. 1990. Activated human monocytes oxidize low-density lipoprotein by a lipoxygenase-dependent pathway. *J. Immunol.* 145:254–259.

Nagelin, M.H., S. Srinivasan, J. Lee, J.L. Nadler, and C.C. Hedrick. 2008. 12/15-Lipoxygenase activity increases the degradation of macrophage ATP-binding cassette transporter G1. *Arterioscler. Thromb. Vasc. Biol.* 28:1811–1819.

Natarajan, R., and J.L. Nadler. 2004. Lipid inflammatory mediators in diabetic vascular disease. *Arterioscler. Thromb. Vasc. Biol.* 24:1542–1548.

Ni, W., K. Egashira, S. Kitamoto, C. Kataoka, M. Koyanagi, S. Inoue, K. Imaizumi, C. Akiyama, K.I. Nishida, and A. Takeshita. 2001. New anti-monocyte chemoattractant protein-1 gene therapy attenuates atherosclerosis in apolipoprotein E-knockout mice. *Circulation.* 103:2096–2101.

Reilly, K.B., S. Srinivasan, M.E. Hatley, M.K. Patricia, J. Lannigan, D.T. Bolick, G. Vandenhoff, H. Pei, R. Natarajan, J.L. Nadler, and C.C. Hedrick. 2004. 12/15-Lipoxygenase activity mediates inflammatory monocyte/endothelial interactions and atherosclerosis in vivo. *J. Biol. Chem.* 279:9440–9450.

Sakashita, T., Y. Takahashi, T. Kinoshita, and T. Yoshimoto. 1999. Essential involvement of 12-lipoxygenase in regiospecific and stereospecific oxidation of low density lipoprotein by macrophages. *Eur. J. Biochem.* 265:825–831.

Sano, M., T. Minamino, H. Toko, H. Miyauchi, M. Orimo, Y. Qin, H. Akazawa, K. Tateno, Y. Kayama, M. Harada, et al. 2007. p53-induced inhibition of Hif-1 causes cardiac dysfunction during pressure overload. *Nature.* 446:444–448.

Seiler, A., M. Schneider, H. Forster, S. Roth, E.K. Wirth, C. Culmsee, N. Plesnila, E. Kremmer, O. Radmark, W. Wurst, et al. 2008. Glutathione peroxidase 4 senses and translates oxidative stress into 12/15-lipoxygenase dependent- and AIF-mediated cell death. *Cell Metab.* 8:237–248.

Wen, Y., J. Gu, S.K. Chakrabarti, K. Aylor, J. Marshall, Y. Takahashi, T. Yoshimoto, and J.L. Nadler. 2007. The role of 12/15-lipoxygenase in the expression of interleukin-6 and tumor necrosis factor-alpha in macrophages. *Endocrinology.* 148:1313–1322.

Wen, Y., J. Gu, G.E. Vandenhoff, X. Liu, and J.L. Nadler. 2008. Role of 12/15-lipoxygenase in the expression of MCP-1 in mouse macrophages. *Am. J. Physiol. Heart Circ. Physiol.* 294:H1933–H1938.

Yokoyama, C., F. Shinjo, T. Yoshimoto, S. Yamamoto, J.A. Oates, and A.R. Brash. 1986. Arachidonate 12-lipoxygenase purified from porcine leukocytes by immunoaffinity chromatography and its reactivity with hydroperoxyeicosatetraenoic acids. *J. Biol. Chem.* 261:16714–16721.

Zhu, D., M. Medhora, W.B. Campbell, N. Spitzbarth, J.E. Baker, and E.R. Jacobs. 2003a. Chronic hypoxia activates lung 15-lipoxygenase, which catalyzes production of 15-HETE and enhances constriction in neonatal rabbit pulmonary arteries. *Circ. Res.* 92:992–1000.

Zhu, H., Y. Takahashi, W. Xu, H. Kawajiri, T. Murakami, M. Yamamoto, S. Iseki, T. Iwasaki, H. Hattori, and T. Yoshimoto. 2003b. Low density lipoprotein receptor-related protein-mediated membrane translocation of 12/15-lipoxygenase is required for oxidation of low density lipoprotein by macrophages. *J. Biol. Chem.* 278:13350–13355.

Journal of Molecular and Cellular Cardiology 47 (2009) 664–675

Contents lists available at ScienceDirect

Journal of Molecular and Cellular Cardiology

journal homepage: www.elsevier.com/locate/yjmcc

Original article

Interaction of myocardial insulin receptor and IGF receptor signaling in exercise-induced cardiac hypertrophy

Hiroyuki Ikeda [a,b], Ichiro Shiojima [a,c], Yukako Ozasa [a], Masashi Yoshida [a], Martin Holzenberger [d], C. Ronald Kahn [e], Kenneth Walsh [f], Takashi Igarashi [b], E. Dale Abel [g], Issei Komuro [a,c,*]

[a] Department of Cardiovascular Science and Medicine, Chiba University Graduate School of Medicine, Chiba, Japan
[b] Department of Pediatrics, University of Tokyo Graduate School of Medicine, Tokyo, Japan
[c] Department of Cardiovascular Medicine, Osaka University Graduate School of Medicine, Suita, Japan
[d] INSERM UMR893, Saint-Antoine Hospital, Paris, France
[e] Joslin Diabetes Center and Department of Medicine, Harvard Medical School, Boston, MA, USA
[f] Molecular Cardiology, Whitaker Cardiovascular Institute, Boston University School of Medicine, Boston, MA, USA
[g] Program in Molecular Medicine and Division of Endocrinology, Metabolism, and Diabetes, University of Utah School of Medicine, Salt Lake City, UT, USA

ARTICLE INFO

Article history:
Received 14 April 2009
Received in revised form 9 August 2009
Accepted 25 August 2009
Available online 8 September 2009

Keywords:
Insulin-like growth factor receptor
Insulin receptor
Exercise
Cardiac hypertrophy
Tyrosine phosphorylation

ABSTRACT

Insulin-like growth factor-1 (IGF-1) signaling has recently been implicated in the development of cardiac hypertrophy after long-term endurance training, via mechanisms that may involve energetic stress. Given the potential overlap of insulin and IGF-1 signaling we sought to determine if both signaling pathways could contribute to exercise-induced cardiac hypertrophy following shorter-term exercise training. Studies were performed in mice with cardiac-specific IGF-1 receptor (IGF1R) knockout (CIGFRKO), mice with cardiac-specific insulin receptor (IR) knockout (CIRKO), CIGFRKO mice that lacked one IR allele in cardiomyocytes (IGFR−/−IR+/−), and CIRKO mice that lacked one IGF1R allele in cardiomyocytes (IGFR+/−IR−/−). Intravenous administration of IGF-1 or 75 hours of swimming over 4 weeks increased IGF1R tyrosine phosphorylation in the heart in control and CIRKO mice but not in CIGFRKO mice. Intriguingly, IR tyrosine phosphorylation in the heart was also increased following IGF-1 administration or exercise training in control and CIGFRKO mice but not in CIRKO mice. The extent of cardiac hypertrophy following exercise training in CIGFRKO and CIRKO mice was comparable to that in control mice. In contrast, exercise-induced cardiac hypertrophy was significantly attenuated in IGFR−/−IR+/− and IGFR+/−IR−/− mice. Thus, IGF-1 and exercise activates both IGF1R and IR in the heart, and IGF1R- and IR-mediated signals may serve redundant roles in the hypertrophic responses of the heart to exercise training.

1. Introduction

Postnatal myocardial growth is primarily achieved through hypertrophy of individual myocytes [1]. In addition to normal heart growth during postnatal development, heart size increases in response to various forms of both extrinsic and intrinsic stimuli [2], and these hypertrophic responses are classified either as "pathological" or "physiological." Pathological cardiac hypertrophy is frequently associated with contractile dysfunction and histological pathology such as interstitial fibrosis, and is typically observed in patients with hypertension, myocardial infarction, and valvular heart diseases. On the other hand, physiological cardiac hypertrophy is characterized by normal or enhanced contractility and normal cardiac architecture, as typically observed in trained athletes [3,4]. Notably, exercise training is beneficial in a selected population of heart failure patients [5] and reverses molecular and functional abnormalities of the heart in animal models of pathological hypertrophy [6–8]. Thus, promoting physiological cardiac hypertrophy may be one of the therapeutic options for heart diseases.

The insulin-like growth factor-1 (IGF-1)–phosphatidylinositol 3-kinase (PI3K)–Akt pathway has been implicated in the development of exercise-induced cardiac hypertrophy [9,10]. Increased cardiac IGF-1 formation is associated with physiological hypertrophy in athletes [11], and exercise training increases IGF-1 mRNA expression in rat hearts [12]. Overexpression of IGF-1 in the heart in transgenic mice induces physiological cardiac hypertrophy in the early phases of postnatal development [13], and IGF-1 receptor (IGF1R) overexpression in the heart results in physiological cardiac hypertrophy associated with activation of the PI3K-Akt pathway [14]. Overexpression of a constitutively active p110α PI3K results in physiological cardiac hypertrophy [15], and exercise-induced hypertrophy is completely abolished by dominant-negative p110α overexpression [14,16]. Short-term or moderate levels of Akt1 overexpression in the heart induces physiological cardiac hypertrophy [17,18], whereas development of exercise-induced cardiac hypertrophy is blunted in Akt1 knockout mice [19].

* Corresponding author. Department of Cardiovascular Science and Medicine, Chiba University Graduate School of Medicine, Chiba, Japan.
E-mail address: komuro-tky@umin.ac.jp (I. Komuro).

0022-2828/$ – see front matter © 2009 Elsevier Inc. All rights reserved.
doi:10.1016/j.yjmcc.2009.08.028

These results collectively suggest that IGF-1 or IGF1R is sufficient whereas PI3K–Akt pathway is both necessary and sufficient to induce physiological cardiac hypertrophy. A recent study in mice with cardiomyocyte-restricted deletion of IGF1R suggested that cardiac IGF1R signaling could modulate exercise-induced cardiac hypertrophy [20]. In this study, 96 hours of swim training over 5 weeks led to increased AMPK activation in IGF1R-deficient hearts, and AMPK activation was postulated to have a negative impact on cardiac hypertrophy. Insulin receptor (IR)-mediated signals have also been implicated in the regulation of cardiac growth and function. Cardiac-specific IR knockout (CIRKO) mice exhibit small heart size with mildly impaired contractility and reduced Akt activity [21,22], suggesting that IR-mediated signals could potentially play a role in exercise-induced physiological hypertrophy.

To elucidate the role of IGF1R and IR in the development of exercise-induced cardiac hypertrophy, we subjected cardiac-specific IGF1R knockout (CIGFRKO) mice and CIRKO mice to 75 hours of swimming over 4 weeks. Although both CIGFRKO mice and CIRKO mice developed exercise-induced cardiac hypertrophy to the level comparable to their wild type littermates, deletion of a single *Ir* or a single *Igf1r* allele on CIGFRKO or CIRKO background, respectively, blunted hypertrophic responses to exercise. We also observed that tyrosine phosphorylation of both IGF1R and IR was increased in the heart after intravenous IGF-1 administration or exercise training. Thus, IGF-1 and exercise may activate both IGF1R and IR in the heart, and IGF1R- and IR-mediated signals may play redundant roles in the development of cardiac hypertrophy in response to exercise training.

2. Materials and methods

2.1. Animals, exercise training, and IGF-1 administration

CIGFRKO mice were initially generated by crossing $Igf1r^{flox/flox}$ mice [23] with α-myosin heavy chain (αMHC)-Cre transgenic mice [24]. Subsequent maintenance of CIGFRKO line was done by crossing CIGFRKO mice ($Igf1r^{flox/flox}Cre^{+/-}$) with $Igf1r^{flox/flox}Cre^{-/-}$ mice. CIRKO mice were generated as described previously [21]. Subsequent maintenance of CIRKO line was done by crossing CIRKO mice ($Ir^{flox/flox}Cre^{+/-}$) with $Ir^{flox/flox}Cre^{-/-}$ mice. Cardiac-specific $Igf1r-/-Ir+/-$ mice and $Igf1r+/-Ir-/-$ mice were generated by crossing $Igf1r^{flox/flox}Ir^{flox/flox}Cre^{-/-}$ mice with CIGFRKO mice ($Igf1r^{flox/flox}Ir^{+/+}Cre^{+/-}$) and CIRKO mice ($Igf1r^{+/+}Ir^{flox/flox}Cre^{+/-}$), respectively. Animals were on a mixed background of C57BL/6J, 129Sv, and FVB, and littermates that contain the same combination of *Igf1r*/*Ir* alleles but do not contain αMHC-Cre transgene were used as wild type controls in each study (Supplementary Fig. S1). Genotyping was performed as described [21,25].

Swimming training was performed in 10-week-old male mice as described previously [26]. Swimming sessions were done twice a day for 28 days. The first 7 days consisted of a training period in which one session was 20 min long on the first day and it was increased by 10 min per day. On the subsequent 21 days, two sessions of 90 min swimming were done. After the final swimming session, mice were overnight fasted and sacrificed. M-mode tracings of left ventricular wall motion at the level of papillary muscle were obtained using Vevo 660 Imaging system (Visual Sonic) with a 25-MHz transducer. For IGF-1 or insulin administration, mice were overnight fasted and anesthetized with pentobarbital, and IGF-1 (Fujisawa Co., Japan) or insulin (Lilly Co., Japan) was intravenously administered. Animals were sacrificed 5 minutes after IGF-1 or insulin administration. All animal procedures were performed with the approval of the Institutional Animal Care and Use Committee of Chiba University.

2.2. Histological analysis

Hearts were fixed and embedded in paraffin for histological analyses. Serial sections of 4 μm were stained with hematoxylin and eosin (HE) for morphological analysis and Masson's trichrome (MT) for detection of fibrosis. For measurements of myocyte cross-sectional area, immunohistochemistry with anti-dystrophin antibody (Novocastra Laboratories, Newcastle, UK) was performed to visualize myocyte membranes. The sections were reacted with anti-dystrophin

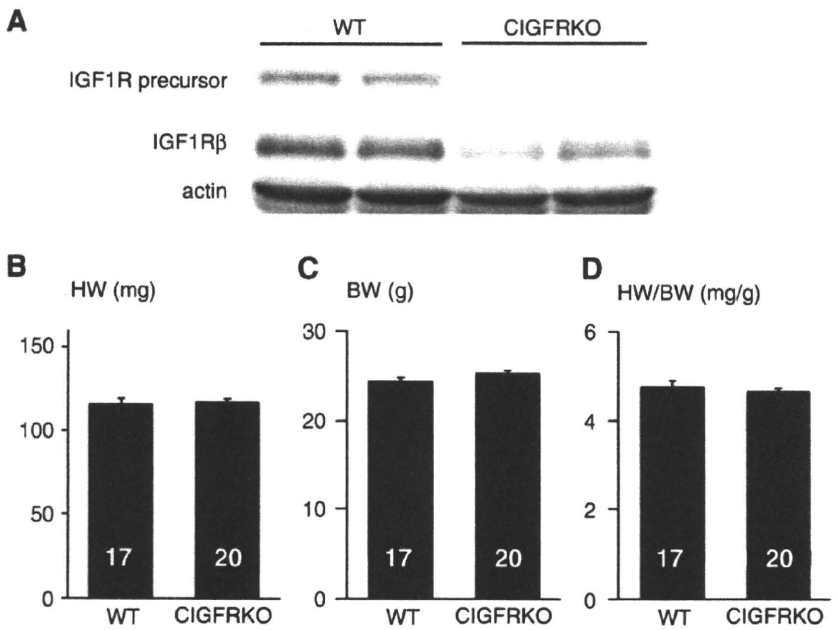

Fig. 1. CIGFRKO mice exhibit no obvious cardiac phenotype at baseline. (A) Expression of IGF1R precursor protein and IGF1R β subunit protein (IGF1Rβ) as revealed by Western blot analysis of whole heart lysates. Actin served as internal control. (B–D) HW (B), BW (C), and HW/BW ratio (D) of WT and CIGFRKO mice at 10 weeks of age. The number of mice analyzed is shown in the bar.

antibody at 1:20 and visualized by ABC method. Suitable cross-sections for measurements were defined as having round-to-oval membrane staining using ImageJ software. At least 200 myocytes were measured in each sample.

2.3. Western blot analysis and immunoprecipitation

Total protein lysate was extracted from heart tissue and SDS–PAGE was performed as described previously [22]. Anti-IGF1Rβ, anti-IRβ, and anti-phosphotyrosine (PY20) antibodies were from Santa Cruz Biotechnology (Santa Cruz, CA), and anti-actin antibody was from Sigma (St. Louis, MO). For immunoprecipitation, total heart lysates (500 μg protein) were precleared with protein G-agarose beads for an hour before incubation with the indicated antibody (1 μg) overnight at 4 °C. Protein G-agarose beads were added for 3 hours and immunoprecipitates were washed three times in lysis buffer, eluted in 2×SDS buffer and subjected to SDS–PAGE.

2.4. Statistical analysis

Data are shown as mean ± SEM. Statistical significance was determined by Student's t test or Welch's test. P values of <0.05 were considered to be statistically significant.

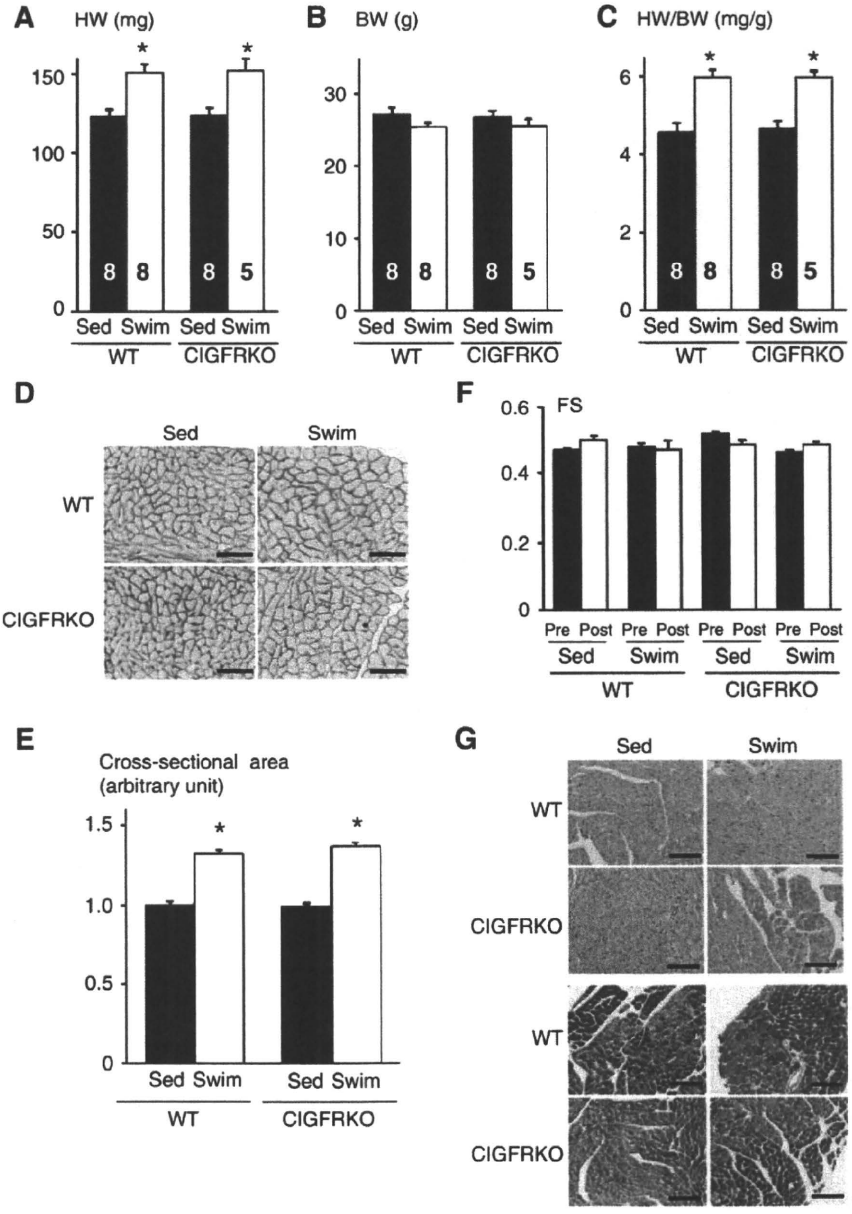

Fig. 2. CIGFRKO mice develop physiological cardiac hypertrophy in response to exercise training. (A–C) HW (A), BW (B), and HW/BW ratio (C) of WT and CIGFRKO mice. *$p<0.05$ versus Sed group of the same genotype. The number of mice analyzed is shown in the bar. (D) Immunohistochemistry with anti-dystrophin antibody. Scale bar = 50 μm. (E) Myocyte cross-sectional area of WT and CIGFRKO mice. *$p<0.05$ versus Sed group of the same genotype. (F) Left ventricular contractile function as assessed by echocardiographic measurement of fractional shortening (FS). Pre and Post represent before and after exercise, respectively. (G) Histological analysis with HE (upper panel) and Masson's trichrome (MT) (lower panel) staining. Scale bar = 100 μm. Sed and Swim represent a sedentary and a swimming group, respectively.

3. Results

3.1. CIGFRKO mice exhibit no cardiac phenotype at baseline

CIGFRKO mice were initially generated by crossing *Igf1r*$^{flox/flox}$ animals with αMHC-Cre transgenic mice, and compared with wild type controls. Western blot analysis of heart lysate revealed that the expression levels of IGF1R precursor protein and IGF1R β subunit protein were reduced, and small amount of proteins detected by western blots were considered to be derived from non-myocytes in the heart (Fig. 1A). At 10 weeks of age, there was no significant difference in heart weight (HW), body weight (BW), heart weight (HW)/BW ratio, and cardiac function as assessed by echocardiography between CIGFRKO mice and wild type (WT) littermates (Figs. 1B–D, and data not shown). Similar results were obtained in other ages. Thus, CIGFRKO mice exhibit no obvious cardiac phenotype at baseline.

3.2. Deletion of *Igf1r* in cardiac myocytes does not attenuate exercise-induced physiological cardiac hypertrophy

Lack of obvious cardiac phenotype in CIGFRKO mice at baseline prompted us to investigate the effect of *Igf1r* deletion on hypertrophic responses of the heart to exercise training. After 75 hours of swimming over 4 weeks, WT and CIGFRKO mice developed similar degrees of cardiac hypertrophy as measured by HW and HW/BW ratio (Figs. 2A-C). The fold increase in myocyte cross-sectional area was also comparable between WT and CIGFRKO animals (Figs. 2D and E). Left ventricular contractile function as measured by echocardiography did not differ between WT and CIGFRKO mice (Fig. 2F), and histological analyses revealed that there was no interstitial fibrosis or myocyte disarray in the hearts of WT and CIGFRKO mice (Fig. 2G). The presence of Cre recombinase in the heart did not affect the extent of hypertrophy or contractile function following exercise training (Supplementary Fig. S2). These results collectively suggest that exercise-induced physiological cardiac hypertrophy may develop normally in the absence of IGF1R-mediated signals in cardiac myocytes.

3.3. IR is phosphorylated by IGF-I in the hearts of WT and CIGFRKO mice

Since IGF-1 signaling has been implicated in the development of physiological cardiac hypertrophy, the above-mentioned results were somewhat unexpected. We first examined whether IGF1R-mediated signals were disrupted in cardiac myocytes of CIGFRKO mice. Western blot analysis of whole heart extracts revealed that, although IGF1R protein levels were upregulated after exercise training in the hearts of WT mice, the expression levels of IGF1R remained at low levels both in sedentary and swim-trained CIGFRKO hearts (Fig. 3A). Tyrosine phosphorylation levels of IGF1R and IR were also examined in the heart of WT and CIGFRKO mice after exercise training. Exercise training increased phosphorylation levels of both IGF1R and IR in the heart of WT mice. Increased phosphorylation levels of IGF1R could be in part attributed to upregulation of IGF1R protein levels following exercise training. As expected, IGF1R phosphorylation but not IR phosphorylation was blunted in the heart of CIGFRKO animals (Fig. 3B). IGF1R tyrosine phosphorylation levels were also examined in the hearts of WT and CIGFRKO mice after intravenous IGF-1 administration. Phosphotyrosine blot after IGF1R immunoprecipitation

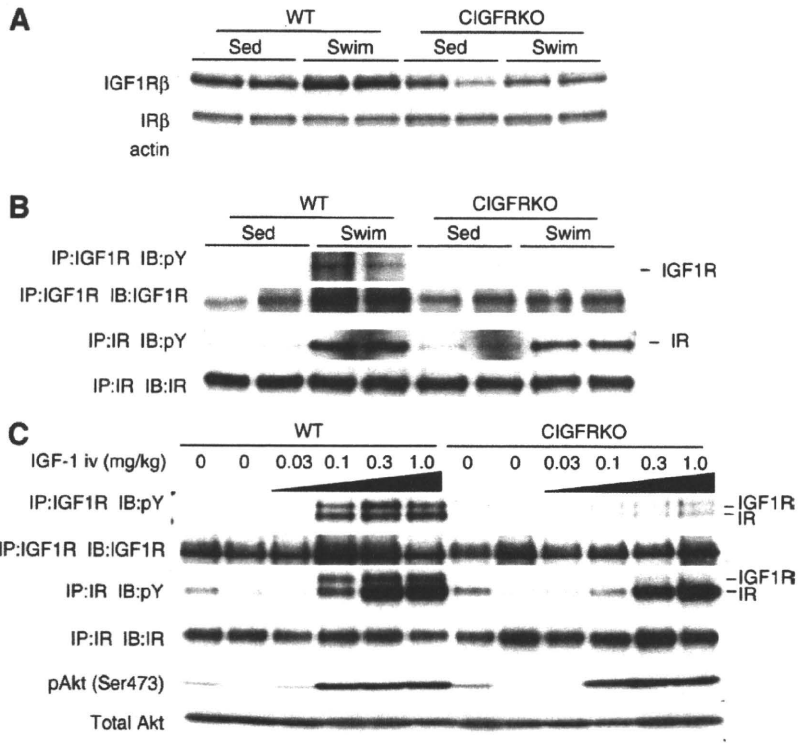

Fig. 3. Western blot analysis of CIGFRKO heart extracts after exercise or IGF-I administration. (A) Expression of IGF1R β subunit protein (IGF1Rβ) and IR β subunit protein (IRβ) in the heart of WT and CIGFRKO mice. Sed and Swim represent a sedentary and a swimming group, respectively. (B) Tyrosine phosphorylation levels of IGF1R and IR following exercise training. pY represents anti-phosphotyrosine antibody. IP and IB represent immunoprecipitation and immunoblot, respectively. (C) Tyrosine phosphorylation levels of IGF1R/IR and activation of Akt in the heart of WT and CIGFRKO mice 5 minutes after IGF-1 administration. There are some IGF1R bands in the immunoprecipitates of IR and vice versa, possibly due to antibody cross-reactivity. pY represents anti-phosphotyrosine antibody. IP and IB represent immunoprecipitation and immunoblot, respectively.

revealed that tyrosine phosphorylation of IGF1R was markedly reduced in CIGFRKO hearts when compared to that of WT hearts (Fig. 3C, upper panel). These findings strongly suggest that IGF1R-mediated signaling is functionally disrupted in cardiac myocytes of CIGFRKO animals. In the same experimental condition, phospho-tyrosine blot after IR immunoprecipitation revealed significant tyrosine phosphorylation of IR both in WT and CIGFRKO hearts after IGF-1 administration (Fig. 3C, middle panel), and phospho-Akt levels in the heart were comparable between WT and CIGFRKO animals (Fig. 3C, lower panel). These observations collectively suggest that IR activated by IGF-1 in part mediates exercise-induced physiological cardiac hypertrophy and that IR compensates for the loss of IGF1R-mediated signaling in the hearts of CIGFRKO mice following exercise training.

3.4. Deletion of Ir in cardiac myocytes does not attenuate exercise-induced physiological cardiac hypertrophy

To test the hypothesis that IR mediates exercise-induced physiological cardiac hypertrophy, CIRKO mice and wild type littermates were subjected to exercise training. After 75 hours of swimming, WT and CIRKO mice exhibited similar degrees of cardiac hypertrophy as

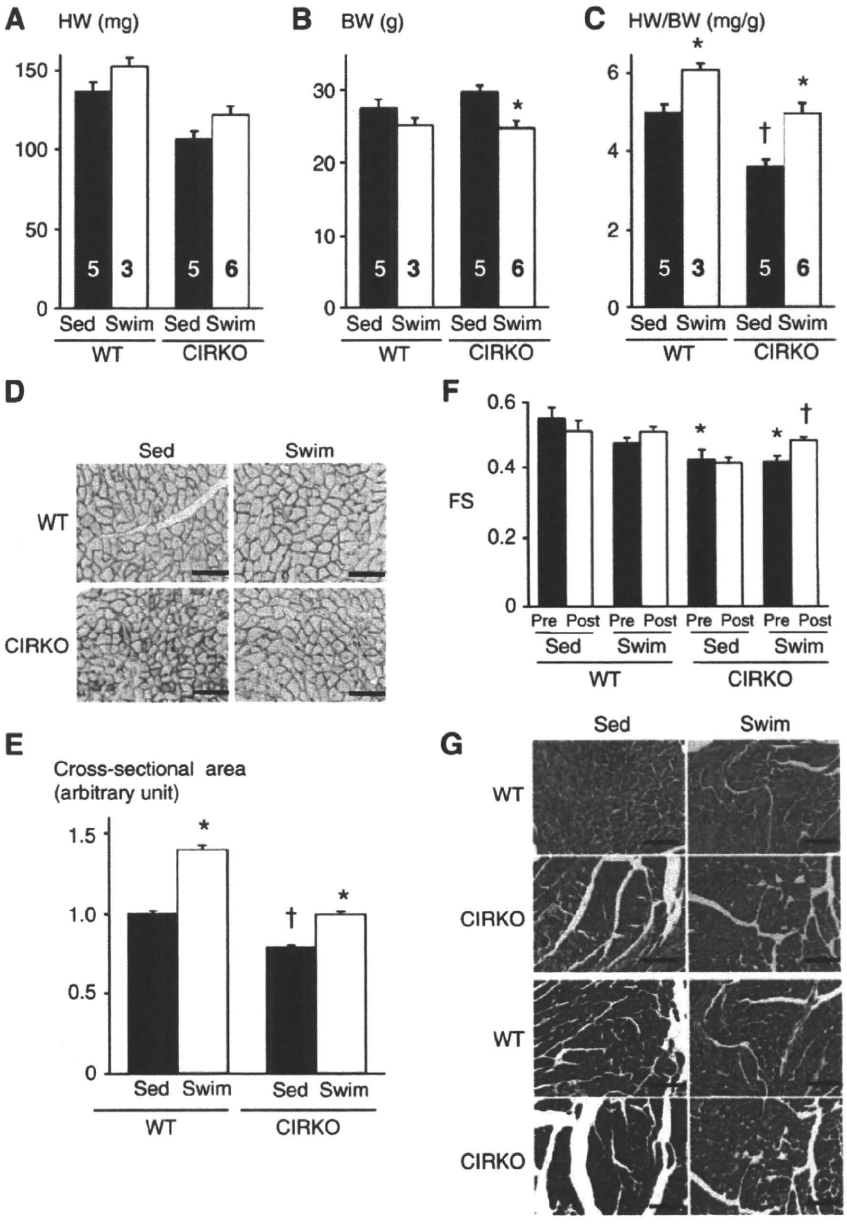

Fig. 4. CIRKO mice develop physiological cardiac hypertrophy in response to exercise training. (A–C) HW (A), BW (B), and HW/BW ratio (C) of WT and CIRKO mice. *p<0.05 versus Sed group of the same genotype, †p<0.05 versus WT Sed group. The number of mice analyzed is shown in the bar. (D) Immunohistochemistry with anti-dystrophin antibody. Scale bar = 50 μm. (E) Myocyte cross-sectional area of WT and CIRKO mice. *p<0.05 versus Sed group of the same genotype. †p<0.05 versus WT Sed group. (F) Left ventricular contractile function as assessed by echocardiographic measurement of fractional shortening (FS). Pre and Post represent before and after exercise, respectively. *p<0.05 versus WT Sed Pre group, †p<0.05 versus CIRKO Swim Pre group. (G) Histological analysis with HE (upper panel) and Masson's trichrome (MT) (lower panel) staining. Scale bar = 100 μm. Sed and Swim represent a sedentary and a swimming group, respectively.

measured by HW (12% versus 14%) and HW/BW ratio (22% versus 38%) (Figs. 4A–C). The fold increase in myocyte cross-sectional area was also significant in WT and CIGFRKO animals (40% and 27%, respectively) (Figs. 4D and E). The relatively enhanced response in HW/BW ratio following exercise was considered to be due to a significant decrease in BW in CIRKO mice following exercise training (Fig. 4B). Interestingly, left ventricular contractile function as assessed by fractional shortening was slightly impaired in CIRKO mice, which was ameliorated by exercise training (Fig. 4F). There was no sign of pathology in histological examination both in WT or CIRKO hearts (Fig. 4G). Thus, exercise-induced physiological cardiac hypertrophy develops normally even in the absence of IR-mediated signals in cardiac myocytes.

Western blot analysis of whole heart extracts revealed that the expression levels of IGF1R were increased in CIRKO hearts at the sedentary state compared to those of WT hearts, and further upregulated after exercise both in WT and CIRKO hearts (Fig. 5A). Tyrosine phosphorylation levels of IGF1R were upregulated both in WT and CIRKO hearts after exercise training, whereas those of IR were upregulated in WT hearts but not in CIRKO hearts (Fig. 5B). When IGF-1 was intravenously administered, phosphotyrosine blot after IGF1R immunoprecipitation revealed that tyrosine phosphorylation of IGF1R was comparable between CIRKO hearts and WT hearts (Fig. 5C, upper panel), whereas phosphotyrosine blot after IR immunoprecipitation revealed that IR tyrosine phosphorylation by IGF-I was markedly reduced in CIRKO hearts (Fig. 5C, middle panel). Phospho-Akt levels in the heart were comparable between WT and CIRKO animals (Fig. 5C, lower panel). These observations indicate that IR-mediated signals are dispensable for the development of exercise-induced physiological cardiac hypertrophy.

3.5. Combined deletion of *Igf1r* and *Ir* attenuates exercise-induced physiological cardiac hypertrophy

The observation that the deletion of either *Igf1r* alone or *Ir* alone in cardiac myocytes does not attenuate swimming-induced cardiac hypertrophy suggests that IGF1R- and IR-mediated signals could compensate for each other during the development of exercise-induced physiological cardiac growth. To test this hypothesis, we generated compound mutants of *Igf1r* and *Ir* genes in the heart. Homozygous deletion of both genes in cardiac myocytes resulted in severe heart failure and early postnatal lethality (data not shown), consistent with a previous report in which *Igf1r* and *Ir* genes were disrupted in cardiac and skeletal muscle cells [27]. We therefore analyzed mice lacking two *Igf1r* alleles and one *Ir* allele (IGF1R−/−IR+/−) or mice lacking one *Igf1r* allele and two *Ir* alleles (IGF1R+/−IR−/−) in cardiac myocytes.

At sedentary state, HW and HW/BW ratio of IGF1R−/−IR+/− mice was comparable to that of WT mice. When these animals were subjected to 75 hours of swimming, the increase in HW and HW/BW ratio was significantly reduced in IGF1R−/−IR+/− mice compared to WT mice (Figs. 6A–C). The increase in myocyte cross-sectional area was also significantly reduced in IGF1R−/−IR+/− animals compared to WT littermates (Figs. 6D and E). Left ventricular contractile function was not affected by gene deletion and/or exercise training (Fig. 6F), and there was no pathological finding on histology (Fig. 6G). Western blot analysis of whole heart extracts revealed that the expression levels of IR were slightly reduced in IGF1R−/−IR+/− hearts and were not altered by exercise (Fig. 7A). When IGF-1 was intravenously administered, tyrosine phosphorylation of IGF1R was markedly reduced (Fig. 7B, upper panel) and that of IR was also

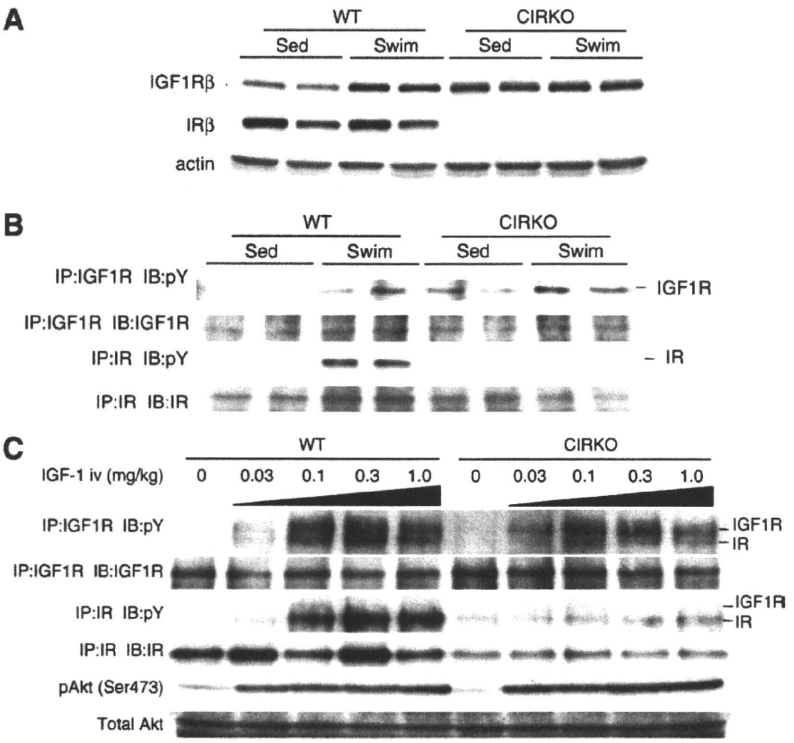

Fig. 5. Western blot analysis of CIRKO heart extracts after exercise or IGF-1 administration. (A) Expression of IGF1R β subunit protein (IGF1Rβ) and IR β subunit protein (IRβ) in the heart of WT and CIRKO mice. Sed and Swim represent a sedentary and a swimming group, respectively. (B) Tyrosine phosphorylation levels of IGF1R an IR following exercise training. pY represents anti-phosphotyrosine antibody. IP and IB represent immunoprecipitation and immunoblot, respectively. (C) Tyrosine phosphorylation levels of IGF1R/IR and activation of Akt in the heart of WT and CIRKO mice 5 minutes after IGF-1 administration. There are some IGF1R bands in the immunoprecipitates of IR and vice versa, possibly due to antibody cross-reactivity. pY represents anti-phosphotyrosine antibody. IP and IB represent immunoprecipitation and immunoblot, respectively.

moderately reduced (Fig. 7B, middle panel). Phospho-Akt levels in the heart were comparable between WT and IGF1R−/−IR+/− animals (Fig. 7B, lower panel).

In contrast to IGF1R−/−IR+/− mice, IGF1R+/−IR−/− mice exhibited small heart size at baseline, and the increase in HW and HW/BW ratio after 4 weeks of swimming was significantly reduced in IGF1R+/−IR−/− mice compared to WT mice (Figs. 8A–C). The increase in myocyte cross-sectional area was also markedly reduced in IGF1R+/−IR−/− animals compared to WT littermates (Figs. 8D and E). Echocardiography revealed a progressive decline in left ventricular contractile function in IGF1R+/−IR−/− mice, which was in part ameliorated by exercise training (Fig. 8F). Histological analysis demonstrated interstitial fibrosis in the heart of IGF1R+/−IR−/− mice at sedentary state, which was markedly reduced by exercise training (Fig. 8G). Western blot analysis of whole heart extracts revealed that the expression levels of IGF1R were upregulated in IGF1R+/−IR−/− hearts at sedentary state but there was no further upregulation of IGF1R expression after swimming (Fig. 9A). When IGF-1 was intravenously administered, tyrosine phosphorylation of IGF1R was moderately reduced (Fig. 9B, upper panel), and that of IR was markedly reduced (Fig. 9B, middle panel). Phospho-Akt levels in the heart were also reduced in the heart of IGF1R+/−IR−/− animals compared to WT mice (Fig. 9B, lower panel). These observations indicate that IR expressed from a single *Ir* allele is sufficient to

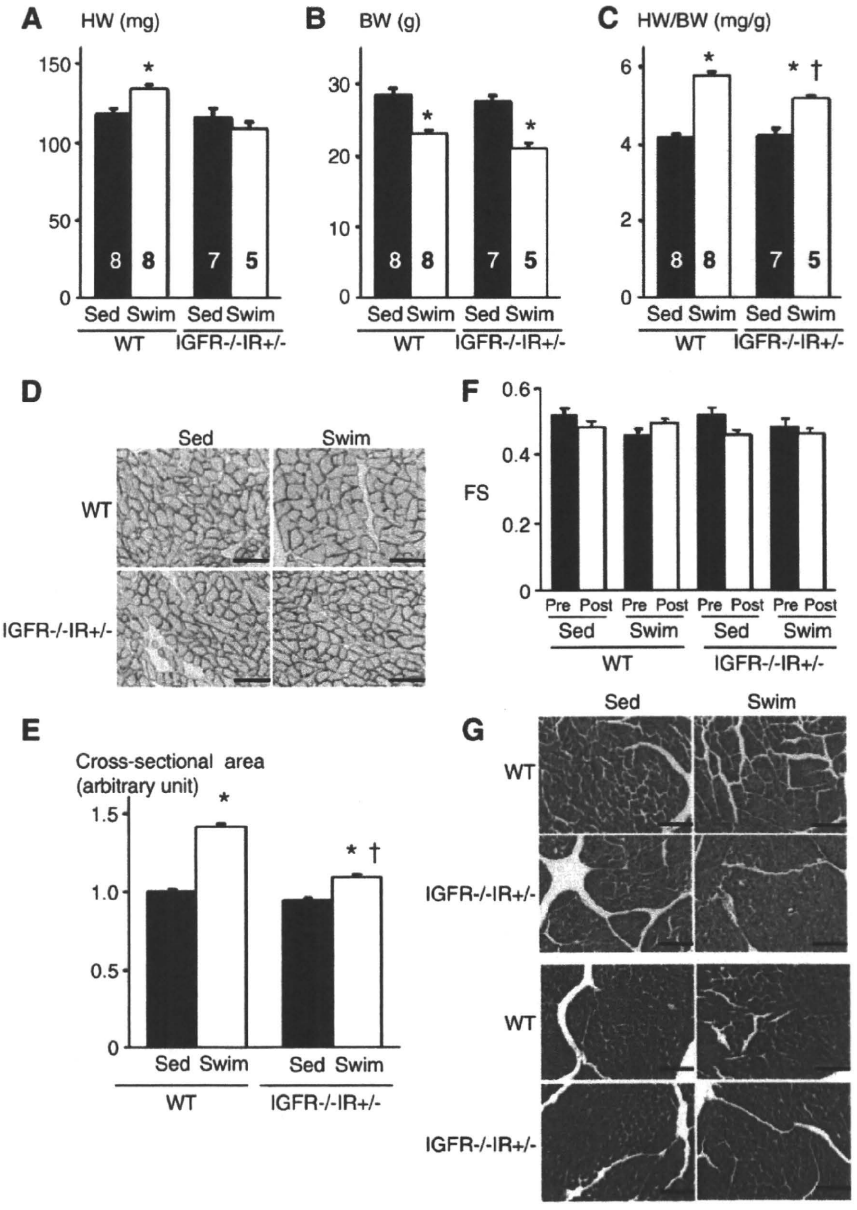

Fig. 6. Exercise-induced physiological cardiac hypertrophy is attenuated in IGF1R−/−IR+/− mice. (A–C) HW (A), BW (B), and HW/BW ratio (C) of WT and IGF1R−/−IR+/− mice. *p<0.05 versus Sed group of the same genotype, †p<0.05 versus WT Swim group. The number of mice analyzed is shown in the bar. (D) Immunohistochemistry with anti-dystrophin antibody. Scale bar = 50 μm. (E) Myocyte cross-sectional area of WT and IGF1R−/−IR+/− mice. *p<0.05 versus Sed group of the same genotype. †p<0.05 versus WT Swim group. (F) Left ventricular contractile function as assessed by echocardiographic measurement of fractional shortening (FS). Pre and Post represent before and after exercise, respectively. (G) Histological analysis with HE (upper panel) and Masson's trichrome (MT) (lower panel) staining. Scale bar = 100 μm. Sed and Swim represent a sedentary and a swimming group, respectively.

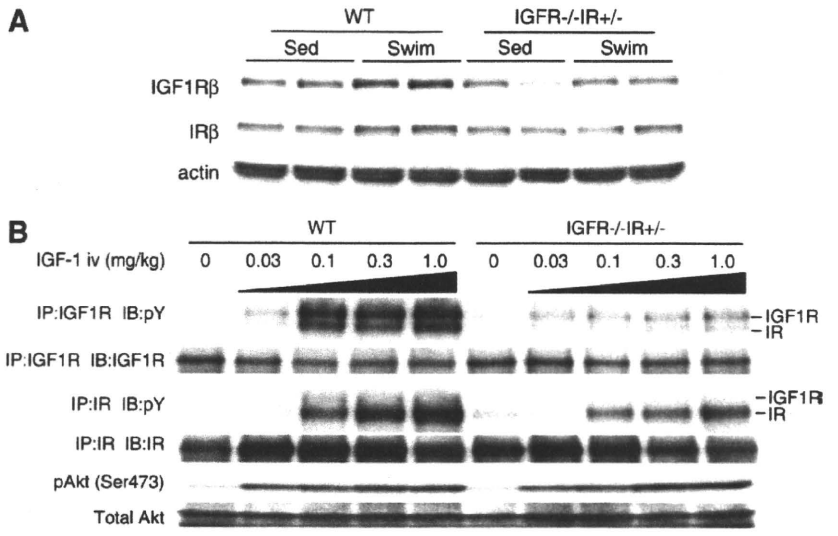

Fig. 7. Western Blot analysis of IGF1R−/−IR+/− heart extracts after exercise or IGF-1 administration. (A) Expression of IGF1R β subunit protein (IGF1Rβ) and IR β subunit protein (IRβ) in the heart of WT and IGF1R−/−IR+/− mice. Sed and Swim represent a sedentary and a swimming group, respectively. (B) Tyrosine phosphorylation levels of IGF1R/IR and activation of Akt in the heart of WT and IGF1R−/−IR+/− mice 5 minutes after IGF-1 administration. There are some IGF1R bands in the immunoprecipitates of IR and vice versa, possibly due to antibody cross-reactivity. pY represents anti-phosphotyrosine antibody. IP and IB represent immunoprecipitation and immunoblot, respectively.

maintain normal postnatal cardiac growth but is insufficient to support the full program of hypertrophic responses to exercise training, whereas IGF1R derived from a single *Igf1r* allele is insufficient both for the maintenance of postnatal cardiac growth/function and for the development of exercise-induced physiological cardiac hypertrophy.

4. Discussion

In the present study, we have dissected the roles of IGF1R and IR in normal postnatal cardiac growth and exercise-induced cardiac hypertrophy. We found that IGF1R and IR have overlapping or redundant functions in these two processes of physiological cardiac growth. We also found that both IGF1R and IR are activated by IGF-1 or exercise, implying that IGF1R- and IR-mediated signals could contribute to hypertrophic responses of the heart to exercise training. These results suggest the existence of a complex signaling network involving IGF1R, IR, and their ligands in the regulation and maintenance of cardiac growth and function (Fig. 10).

Biological actions of insulin and IGF-1 are transduced by IR and IGF1R. These receptors are highly homologous and exist as $\alpha_2\beta_2$ heterodimers, with two extracellular ligand-binding α subunits and two transmembrane β subunits that contain tyrosine kinase domains [28]. There also exists a hybrid IR–IGF1R receptor formed by IR α–β heterodimer and IGF1R α–β heterodimer, which preferentially binds to IGF-1 but not to insulin [29]. Under normal conditions, insulin and IGF-1 signal primarily through their cognate receptors. Thus, insulin signaling acutely regulates glucose metabolism, whereas IGF-1 signaling regulates embryonic and postnatal body/organ size. This notion is supported by distinct phenotypes of IR and IGF1R knockout mice: IR-deficient mice are perinatally lethal due to severe ketoacidosis, whereas IGF1R-deficient mice exhibit severe growth retardation (~45% of normal size) [30]. However, it is probably an oversimplification to view that IR mediates metabolic actions and IGF1R mediates growth. Indeed, IR-deficient mice are slightly smaller than wild type mice (~90% of normal size), and combined deletion of IR and IGF1R results in more severe growth retardation (~30% of normal size) than IGF1R single deletion [30]. Thus, IR and IGF1R have functional redundancies in mediating growth promoting effects during embryonic development.

We previously reported that CIRKO mice exhibit a small heart phenotype (~80% of the wild type heart size). Based on the observation that IGF1R-deficient mice show more severe growth retardation than IR-deficient mice [30], we initially hypothesized that IGF1R-mediated signals would play a dominant role over IR-mediated signals in normal postnatal cardiac growth. However, we found that there was no obvious cardiac phenotype in CIGFRKO mice at baseline. Furthermore, simultaneous deletion of *Ir* and *Igf1r* in cardiac myocytes resulted in perinatal lethality with contractile dysfunction and reduced heart size (data not shown). These observations suggest that IR and IGF1R have functional redundancies in mediating postnatal cardiac growth and that IR plays a dominant role over IGF1R in this process. Although the basis for differential contribution of IR and IGF1R to embryonic development (IR<IGF1R) versus postnatal heart growth (IR>IGF1R) is not clear, it may be due to differences in relative expression levels of IR, IGF1R, and their ligands during embryonic versus postnatal development.

The lack of obvious cardiac phenotype in CIGFRKO mice prompted us to investigate the effect of *Igf1r* deletion in the heart under stressed conditions. Previous studies implicated a critical role of IGF-1–PI3K–Akt pathway in the development of exercise-induced physiological cardiac hypertrophy [9,10]. Specifically, gain-of-function studies in transgenic mice revealed that IGF1R is capable of inducing physiological cardiac growth [14]. We therefore hypothesized that hypertrophic responses to exercise training might be impaired in the heart of CIGFRKO mice. Unexpectedly, however, both wild type and CIGFRKO mice developed comparable levels of cardiac hypertrophy in response to swimming training. In addition, IGF-1 administration or exercise training induced extensive tyrosine phosphorylation of IR in the heart of wild type and CIGFRKO mice. On the contrary, insulin administration induced robust phosphorylation of IR but not IGF1R (Supplementary Fig. S3). These findings suggest that both IGF1R and IR can be activated by IGF-1 and may contribute to the development of exercise-induced cardiac hypertrophy in a functionally redundant fashion. This notion was further supported by our studies in CIRKO, IGF1R−/−IR+/−, and IGF1R+/−IR−/− mice, in which combined deletion of *Igf1r* and *Ir* gene in cardiac myocytes attenuated hypertrophic responses of the heart to exercise training whereas deletion of *Ir* gene alone did not. Furthermore, the observation that IGF1R+/−IR−/− mice were more severely impaired in hypertrophic

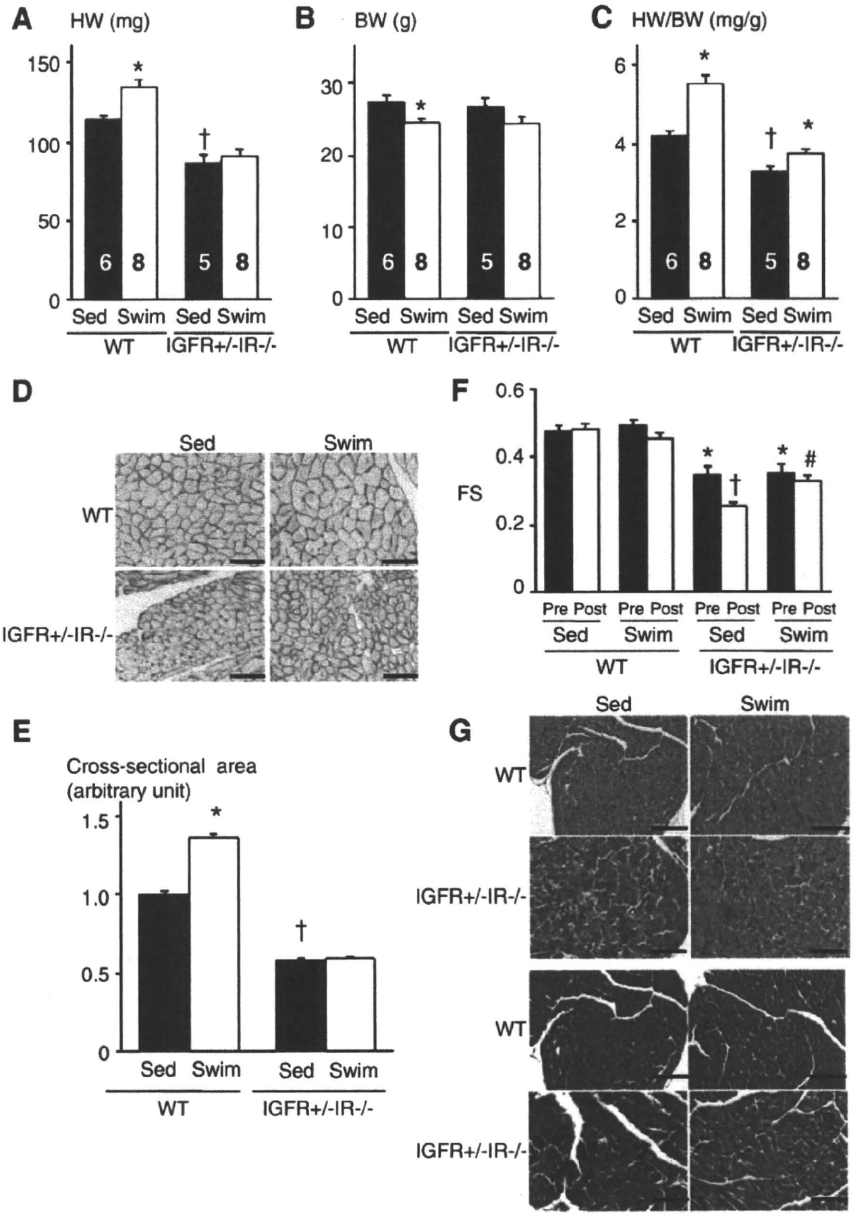

Fig. 8. Exercise-induced physiological cardiac hypertrophy is attenuated in IGF1R+/−IR−/− mice. (A–C) HW (A), BW (B), and HW/BW ratio (C) of WT and IGF1R+/−IR−/− mice. *p<0.05 versus Sed group of the same genotype, †p<0.05 versus WT Sed group. The number of mice analyzed is shown in the bar. (D) Immunohistochemistry with anti-dystrophin antibody. Scale bar = 50 μm. (E) Myocyte cross-sectional area of WT and IGF1R+/−IR−/− mice. *p<0.05 versus WT Sed group. †p<0.05 versus WT Sed group. (F) Left ventricular contractile function as assessed by echocardiographic measurement of fractional shortening (FS). Pre and Post represent before and after exercise, respectively. *p<0.05 versus WT Sed Pre group, †p<0.05 versus IGF1R+/−IR−/− Sed Pre group, #p<0.05 versus IGF1R+/−IR−/− Sed Post group. (G) Histological analysis with HE (upper panel) and Masson's trichrome (MT) (lower panel) staining. Scale bar = 100 μm. Sed and Swim represent a sedentary and a swimming group, respectively.

responses to exercise than IGF1R−/−IR+/− mice suggests that IR-mediated signals might play a dominant role over those mediated by IGF1R in exercise-induced cardiac hypertrophy, as is the case with normal postnatal cardiac growth. Our results also suggest the possibility that the small heart phenotype of CIRKO mice is in part due to the impairment of IR signals activated by IGF-1 or IGF-2 but not by insulin.

The IGF-1–PI3K–Akt pathway has been implicated in physiological cardiac growth. However, the precise mechanism by which this signaling pathway regulates cardiac growth is not completely understood. Although IR appears to be activated by IGF-1 in the heart, the binding affinity of IGF-1 to IR has been reported to be ~100-fold lower relative to that of insulin to IR. One possible mechanism of cross talk between IGF-1 and IR is the ability of IGF1R-IR hybrid receptors to bind to IGF-1 but not to insulin. It was also recently shown that IGF-1 activates IR at physiological concentrations in murine fibroblasts [31]. In this case, IGF-1 selectively activates IRS-2 and the PI3K pathway but not the IRS-1 and ERK pathway. These and other potential mechanisms of IR activation by IGF-1 could contribute to the development of exercise-induced cardiac hypertrophy.

Kim et al. [20] recently reported that exercise-induced cardiac hypertrophy is attenuated in CIGFRKO mice and that activation of AMPK in the heart of CIGFRKO mice is a potential mechanism leading to impaired hypertrophic responses in these animals. However, we could not detect significant differences in cardiac AMPK activity between WT and CIGFRKO mice either before or after exercise. An

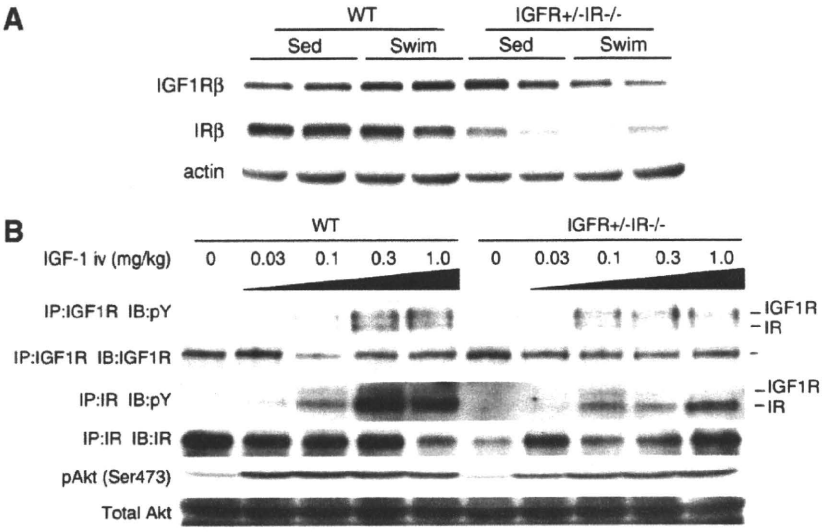

Fig. 9. Western blot analysis of IGF1R+/−IR−/− heart extracts after exercise or IGF-1 administration. (A) Expression of IGF1R β subunit protein (IGF1Rβ) and IR β subunit protein (IRβ) in the heart of WT and IGF1R+/−IR−/− mice. Sed and Swim represent a sedentary and a swimming group, respectively. (B) Tyrosine phosphorylation levels of IGF1R/IR and activation of Akt in the heart of WT and IGF1R+/−IR−/− mice 5 minutes after IGF-1 administration. There are some IGF1R bands in the immunoprecipitates of IR and vice versa, possibly due to antibody cross-reactivity. pY represents anti-phosphotyrosine antibody. IP and IB represent immunoprecipitation and immunoblot, respectively.

important difference between Kim's study and our own is that the study of Kim et al used a more protracted exercise protocol (96 hours total over 5 weeks) at a higher altitude (4000 ft above sea level). This might be the reason for the activation of AMPK in CIGFRKO mice in those studies but not in ours. In addition, Kim et al. [20] reported that Akt activity was not altered between CIGFRKO mice and wild type mice after exercise training, although the degree of exercise-induced cardiac hypertrophy was significantly reduced in CIGFRKO animals. In the present study, although exercise-induced cardiac hypertrophy was impaired in IGF1R−/−IR+/− mice, phospho-Akt levels of IGF1R−/−IR+/− mice were comparable to those of wild type mice (Fig. 7B). Likewise, although exercise-induced cardiac hypertrophy was severely impaired in IGF1R+/−IR−/− mice, phospho-Akt levels in the heart were only slightly impaired in IGF1R+/−IR−/− mice compared to those in wild type mice (Fig. 9B). Thus, the level of activation of Akt does not necessarily correlate with the degree of cardiac hypertrophy in *Igf1r* and *Igf1r/Ir* compound mutant mice. Taken together, these two studies would suggest that deficiency of IGF-1 signaling in the heart does not prevent exercise-induced cardiac hypertrophy on the basis of reduced signaling via the IGF1R to Akt, but may impact cardiac hypertrophy by indirect mechanisms. Our data would suggest that these mechanisms become amplified when insulin and IGF-1 signaling are simultaneously impaired.

In summary, we have demonstrated overlapping roles of IGF1R- and IR-mediated signals in the development of exercise-induced physiological cardiac hypertrophy (Fig. 10). The cross talk between IGF1R- and IR-mediated signals might be in part at the level of ligand-receptor interaction at the cell surface. Further elucidation of the signaling pathways downstream of the insulin and IGF-1 receptors that modulate physiological cardiac hypertrophy might identify novel targets that could be exploited in the management of heart failure, where evidence exists that function and prognosis might be increased by exercise.

Acknowledgments

We thank E. Fujita, R. Kobayashi, and Y. Ishiyama for technical assistance. This work was supported by grants from the Ministry of Education, Culture, Sports, Science and Technology (MEXT) to I.K. and by NIH grant RO1HL070070 to E.D.A.

Appendix A. Supplementary data

Supplementary data associated with this article can be found, in the online version, at doi:10.1016/j.yjmcc.2009.08.028.

References

[1] Pasumarthi KB, Field LJ. Cardiomyocyte cell cycle regulation. Circ Res 2002;90:1044–54.
[2] Olson EN, Schneider MD. Sizing up the heart: development redux in disease. Genes Dev 2003;17:1937–56.
[3] Richey PA, Brown SP. Pathological versus physiological left ventricular hypertrophy: a review. J Sports Sci 1998;16:129–41.
[4] Heineke J, Molkentin JD. Regulation of cardiac hypertrophy by intracellular signalling pathways. Nat Rev Mol Cell Biol 2006;7:589–600.
[5] Coats AJ. Exercise training for heart failure: coming of age. Circulation 1999;99:1138–40.
[6] Konhilas JP, Watson PA, Maass A, Boucek DM, Horn T, Stauffer BL, Luckey SW, Rosenberg P, Leinwand LA. Exercise can prevent and reverse the severity of hypertrophic cardiomyopathy. Circ Res 2006;98:540–8.
[7] McMullen JR, Amirahmadi F, Woodcock EA, Schinke-Braun M, Bouwman RD, Hewitt KA, Mollica JP, Zhang L, Zhang Y, Shioi T, Buerger A, Izumo S, Jay PY, Jennings GL. Protective effects of exercise and phosphoinositide 3-kinase (p110alpha) signaling in dilated and hypertrophic cardiomyopathy. Proc Natl Acad Sci U S A 2007;104:612–7.
[8] Scheuer J, Malhotra A, Hirsch C, Capasso J, Schaible TF. Physiologic cardiac hypertrophy corrects contractile protein abnormalities associated with pathologic hypertrophy in rats. J Clin Invest 1982;70:1300–5.
[9] Shiojima I, Walsh K. Regulation of cardiac growth and coronary angiogenesis by the Akt/PKB signaling pathway. Genes Dev 2006;20:3347–65.
[10] Dorn Jr GW. The fuzzy logic of physiological cardiac hypertrophy. Hypertension 2007;49:962–70.
[11] Neri Serneri GG, Boddi M, Modesti PA, Cecioni I, Coppo M, Padeletti L, Michelucci A, Colella A, Galanti G. Increased cardiac sympathetic activity and insulin-like growth factor-I formation are associated with physiological hypertrophy in athletes. Circ Res 2001;89:977–82.
[12] Scheinowitz M, Kessler-Icekson G, Freimann S, Zimmermann R, Schaper W, Golomb E, Savion N, Eldar M. Short- and long-term swimming exercise training increases myocardial insulin-like growth factor-I gene expression. Growth Horm IGF Res 2003;13:19–25.
[13] Delaughter MC, Taffet GE, Fiorotto ML, Entman ML, Schwartz RJ. Local insulin-like growth factor I expression induces physiologic, then pathologic, cardiac hypertrophy in transgenic mice. FASEB J 1999;13:1923–9.
[14] McMullen JR, Shioi T, Huang WY, Zhang L, Tarnavski O, Bisping E, Schinke M, Kong S, Sherwood MC, Brown J, Riggi L, Kang PM, Izumo S. The insulin-like growth factor 1 receptor induces physiological heart growth via the phosphoinositide 3-kinase (p110alpha) pathway. J Biol Chem 2004;279:4782–93.
[15] Shioi T, Kang PM, Douglas PS, Hampe J, Yballe CM, Lawitts J, Cantley LC, Izumo S. The conserved phosphoinositide 3-kinase pathway determines heart size in mice. EMBO J 2000;19:2537–48.

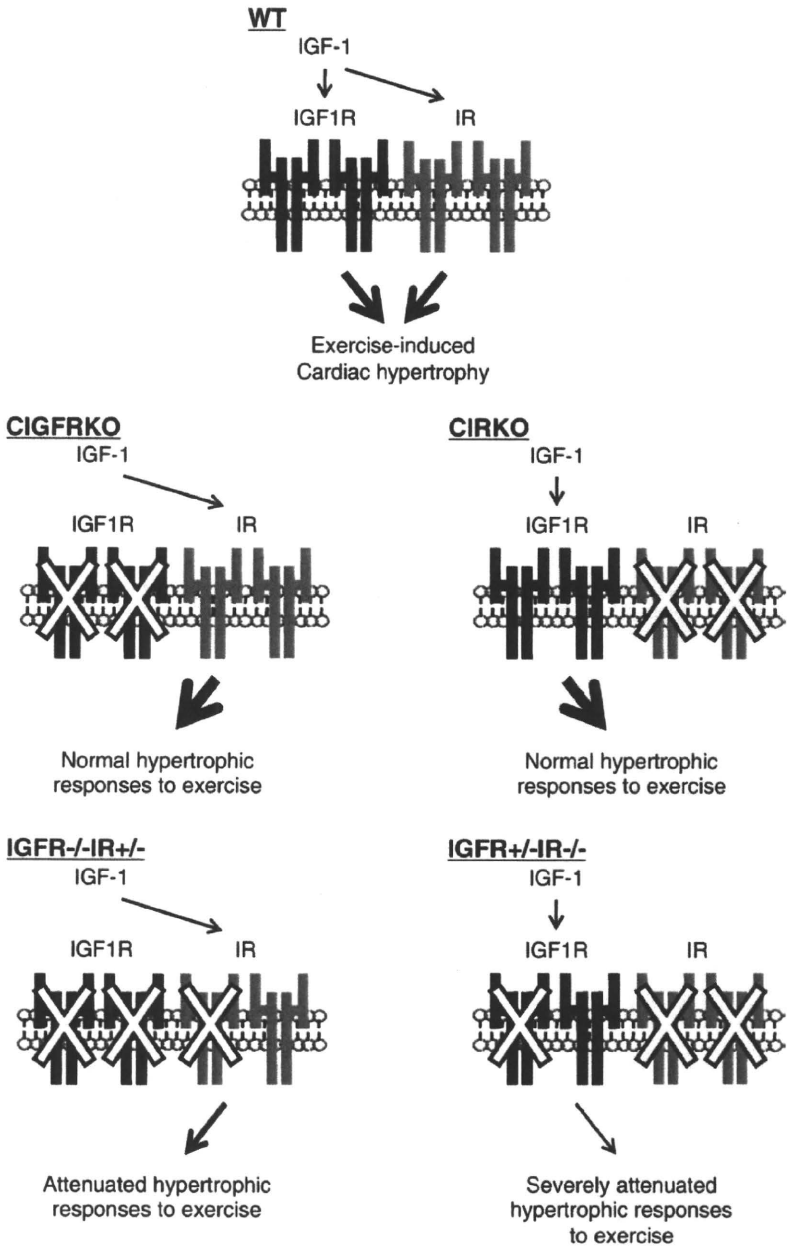

Fig. 10. Schematic illustration of the interaction and cross talk between IGF1R- and IR-mediated signals in exercise-induced cardiac hypertrophy. IGF-1 activates both IGF1R and IR in the heart in response to exercise training. Exercise-induced cardiac hypertrophy develops normally in CIGFRKO mice and CIRKO mice, although combined deletion of two *Igf1r* alleles and one *Ir* allele or one *Igf1r* allele and two *Ir* alleles results in the attenuation of exercise-induced hypertrophy. Thus, exercise-induced cardiac hypertrophy is mediated both by IGF1R- and IR-mediated signals in a redundant fashion. IGF-1 appears to be a major factor that activates both IGF1R and IR. The contribution of insulin in exercise-induced cardiac hypertrophy is not clear from our present study.

[16] McMullen JR, Shioi T, Zhang L, Tarnavski O, Sherwood MC, Kang PM, Izumo S. Phosphoinositide 3-kinase(p110alpha) plays a critical role for the induction of physiological, but not pathological, cardiac hypertrophy. Proc Natl Acad Sci U S A 2003;100:12355–60.
[17] Condorelli G, Drusco A, Stassi G, Bellacosa A, Roncarati R, Iaccarino G, Russo MA, Gu Y, Dalton N, Chung C, Latronico MV, Napoli C, Sadoshima J, Croce CM, Ross Jr J. Akt induces enhanced myocardial contractility and cell size in vivo in transgenic mice. Proc Natl Acad Sci U S A 2002;99:12333–8.
[18] Shiojima I, Sato K, Izumiya Y, Schiekofer S, Ito M, Liao R, Colucci WS, Walsh K. Disruption of coordinated cardiac hypertrophy and angiogenesis contributes to the transition to heart failure. J Clin Invest 2005;115:2108–18.
[19] DeBosch B, Treskov I, Lupu TS, Weinheimer C, Kovacs A, Courtois M, Muslin AJ. Akt1 is required for physiological cardiac growth. Circulation 2006;113: 2097–104.
[20] Kim J, Wende AR, Sena S, Theobald HA, Soto J, Sloan C, Wayment BE, Litwin SE, Holzenberger M, Leroith D, Abel ED. IGF-1 receptor signaling is required for exercise-induced cardiac hypertrophy. Mol Endocrinol 2008;22:2531–43.
[21] Belke DD, Betuing S, Tuttle MJ, Graveleau C, Young ME, Pham M, Zhang D, Cooksey RC, McClain DA, Litwin SE, Taegtmeyer H, Severson D, Kahn CR, Abel ED. Insulin signaling coordinately regulates cardiac size, metabolism, and contractile protein isoform expression. J Clin Invest 2002;109:629–39.
[22] Shiojima I, Yefremashvili M, Luo Z, Kureishi Y, Takahashi A, Tao J, Rosenzweig A, Kahn CR, Abel ED, Walsh K. Akt signaling mediates postnatal heart growth in response to insulin and nutritional status. J Biol Chem 2002;277:37670–7.
[23] Holzenberger M, Leneuve P, Hamard G, Ducos B, Perin L, Binoux M, Le Bouc Y. A targeted partial invalidation of the insulin-like growth factor I receptor gene in mice causes a postnatal growth deficit. Endocrinology 2000;141:2557–66.
[24] Abel ED, Kaulbach HC, Tian R, Hopkins JC, Duffy J, Doetschman T, Minnemann T, Boers ME, Hadro E, Oberste-Berghaus C, Quist W, Lowell BB, Ingwall JS, Kahn BB. Cardiac hypertrophy with preserved contractile function after selective deletion of GLUT4 from the heart. J Clin Invest 1999;104:1703–14.
[25] Leneuve P, Zaoui R, Monget P, Le Bouc Y, Holzenberger M. Genotyping of Cre-lox mice and detection of tissue-specific recombination by multiplex PCR. Biotechniques 2001;31:1156–60,1162.

[26] Oka T, Maillet M, Watt AJ, Schwartz RJ, Aronow BJ, Duncan SA, Molkentin JD. Cardiac-specific deletion of Gata4 reveals its requirement for hypertrophy, compensation, and myocyte viability. Circ Res 2006;98:837–45.
[27] Laustsen PG, Russell SJ, Cui L, Entingh-Pearsall A, Holzenberger M, Liao R, Kahn CR. Essential role of insulin and insulin-like growth factor 1 receptor signaling in cardiac development and function. Mol Cell Biol 2007;27:1649–64.
[28] Taniguchi CM, Emanuelli B, Kahn CR. Critical nodes in signalling pathways: insights into insulin action. Nat Rev Mol Cell Biol 2006;7:85–96.
[29] Slaaby R, Schaffer L, Lautrup-Larsen I, Andersen AS, Shaw AC, Mathiasen IS, Brandt J. Hybrid receptors formed by insulin receptor (IR) and insulin-like growth factor I receptor (IGF-IR) have low insulin and high IGF-1 affinity irrespective of the IR splice variant. J Biol Chem 2006;281:25869–74.
[30] Rother KI, Accili D. Role of insulin receptors and IGF receptors in growth and development. Pediatr Nephrol 2000;14:558–61.
[31] Denley A, Carroll JM, Brierley GV, Cosgrove L, Wallace J, Forbes B, Roberts Jr CT. Differential activation of insulin receptor substrates 1 and 2 by insulin-like growth factor-activated insulin receptors. Mol Cell Biol 2007;27:3569–77.

Cardiac mast cells cause atrial fibrillation through PDGF-A–mediated fibrosis in pressure-overloaded mouse hearts

Chien-hui Liao,[1,2] Hiroshi Akazawa,[1] Masaji Tamagawa,[3] Kaoru Ito,[1] Noritaka Yasuda,[1] Yoko Kudo,[1] Rie Yamamoto,[1] Yukako Ozasa,[1] Masanori Fujimoto,[1] Ping Wang,[1] Hiromitsu Nakauchi,[2] Haruaki Nakaya,[3] and Issei Komuro[1]

[1]Department of Cardiovascular Science and Medicine, Chiba University Graduate School of Medicine, Chiba, Japan. [2]Division of Stem Cell Therapy, Center for Stem Cell and Regenerative Medicine, Institute of Medical Science, University of Tokyo, Tokyo, Japan. [3]Department of Pharmacology, Chiba University Graduate School of Medicine, Chiba, Japan.

Atrial fibrillation (AF) is a common arrhythmia that increases the risk of stroke and heart failure. Here, we have shown that mast cells, key mediators of allergic and immune responses, are critically involved in AF pathogenesis in stressed mouse hearts. Pressure overload induced mast cell infiltration and fibrosis in the atrium and enhanced AF susceptibility following atrial burst stimulation. Both atrial fibrosis and AF inducibility were attenuated by stabilization of mast cells with cromolyn and by BM reconstitution from mast cell–deficient WBB6F1-*Kit*$^{W/W\text{-}v}$ mice. When cocultured with cardiac myocytes or fibroblasts, BM-derived mouse mast cells increased platelet-derived growth factor A (PDGF-A) synthesis and promoted cell proliferation and collagen expression in cardiac fibroblasts. These changes were abolished by treatment with a neutralizing antibody specific for PDGF α-receptor (PDGFR-α). Consistent with these data, upregulation of atrial *Pdgfa* expression in pressure-overloaded hearts was suppressed by BM reconstitution from WBB6F1-*Kit*$^{W/W\text{-}v}$ mice. Furthermore, injection of the neutralizing PDGFR-α–specific antibody attenuated atrial fibrosis and AF inducibility in pressure-overloaded hearts, whereas administration of homodimer of PDGF-A (PDGF-AA) promoted atrial fibrosis and enhanced AF susceptibility in normal hearts. Our results suggest a crucial role for mast cells in AF and highlight a potential application of controlling the mast cell/PDGF-A axis to achieve upstream prevention of AF in stressed hearts.

Introduction

Atrial fibrillation (AF) is a supraventricular arrhythmia that is characterized by rapid and fibrillatory atrial activation with an irregular ventricular response. AF remains the most common arrhythmia encountered in clinical practice and is associated with an increased risk of stroke, heart failure, and overall mortality (1). Several cardiovascular disorders predispose to AF, such as coronary artery disease, valvular heart disease, congestive heart failure, and hypertension, especially when LV hypertrophy is present (1). Recent electrophysiological evidence has indicated that the triggering ectopic foci act on predisposing substrates to initiate single- or multiple-circuit reentry, leading to AF (2). The most important histopathological change in AF is atrial fibrosis (3, 4). Accumulation of ECM proteins has been documented in biopsied specimens of atrium from patients with AF (5), and experimental studies using animal models have indicated that interstitial deposition of dense ECM proteins causes separation between bundles of atrial myocytes and disturbs cell-to-cell impulse propagation (3, 4). In addition, atrial fibrosis potentially exaggerates myocardial ischemia by hampering oxygen diffusion and alters the electrophysical and biomechanical properties of atrial myocytes, allowing the initiation and perpetuation of AF (4). The mechanisms underlying the development of atrial fibrosis in AF remain unclear, but evolving evidence has suggested that inflammation is profoundly implicated in the process of the structural remodeling in the atrium (4, 6). Inflammatory infiltrates were observed in the atrium of AF patients and animal models (7, 8). Furthermore, inflammatory biomarkers such as C-reactive protein were elevated in AF patients and were associated with the presence of AF and the future development of AF (9, 10). However, it remains to be fully elucidated how inflammation is linked to the development of structural remodeling as a susceptible AF substrate in stressed hearts.

Mast cells function as key effector cells during allergic and immune responses through releasing preformed or newly synthesized bioactive products (11). Recent studies have implicated mast cells in inflammation and tissue remodeling (11, 12). Indeed, mast cells reside in many tissues including the heart (13) and participate in the inflammatory process underlying several cardiovascular disorders, such as atherosclerosis (14, 15), aortic aneurysm (16, 17), heart failure (18), viral myocarditis (19), and ventricular arrhythmia during ischemia/reperfusion injury (20). In particular, mast cell–derived IL-6 and IFN-γ have been reported to promote atherosclerosis and abdominal aortic aneurysm (15, 16). Meanwhile, mast cells enhance the fibrogenic process through the release of multiple proteases and inflammatory cytokines in the skin, lung, and kidney (21–24). Here, we demonstrate that mast cells infiltrate the atrium of pressure-overloaded mice and contribute to the pathogenesis of atrial fibrosis and AF susceptibility. Mechanistically, upregulation of PDGF-A mediates the fibrogenic effect of mast cells in promoting AF. These results provide mechanistic insights into the pathogenic role of mast cells in promoting an AF substrate in stressed hearts.

Conflict of interest: The authors have declared that no conflict of interest exists.

Citation for this article: *J. Clin. Invest.* **120**:242–253 (2010). doi:10.1172/JCI39942.